Defence Research and Development Canada
Recherche et développement pour la défense Canada

CAN UNCLASSIFIED

DRDC | RDDC
technologyscience technologie

# Sounding principles for high latitude BLOS HF channels

T.J. Willink
DRDC – Ottawa Research Centre

**Defence Research and Development Canada**
**Reference Document**
DRDC-RDDC-2018-D122
November 2018

CAN UNCLASSIFIED

Canada

## IMPORTANT INFORMATIVE STATEMENTS



Endorsement statement: This publication has been published by the Editorial Office of Defence Research and Development Canada, an agency of the Department of National Defence of Canada. Inquiries can be sent to: Publications.DRDC-RDDC@drdc-rddc.gc.ca.

# Abstract

Beyond-line-of-sight (BLOS) HF communication propagates via the ionosphere; this atmospheric layer is disturbed by geomagnetic activity, causing the received signal to be distorted by Doppler fading and shift. In polar and auroral regions, these Doppler effects can be quite severe, affecting the reliability and robustness of communication links. Temporal dispersion causes multipath spread on each mode, and multiple modes may be observed resulting from reflection at different ionospheric layers and/or multi-hop paths that include reflection from the Earth. The propagation parameters are quite dynamic, with trends observed diurnally, seasonally and over the multi-year sunspot cycle, and vary by operating frequency. To design and evaluate radio technology for these conditions, it is necessary to characterise the propagation parameters on a variety of communication links at different times. Measurement campaigns to obtain the relevant ranges of parameters require carefully-designed channel sounders. Pseudo-noise sequences with pulse-compression characteristics are suitable for extracting the channel responses with a minimal amount of signal processing. Herein, several periodic and aperiodic pseudo-noise sequences are evaluated over a wide range of propagation conditions, obtained from previous high-latitude sounding campaigns. It is found that short aperiodic sequences are the most reliable selection: although they have limited processing gain, they are short enough to limit distortions due to Doppler fading and shift, and their implementation can be tuned to achieve appropriate trade-offs to measure the desired range of multipath and Doppler spreads. Other components to the sounding waveform might include capabilities to resolve ambiguities in delay and frequency.



# Résumé

Les communications HF (haute fréquence) au-delà de la ligne de visée se propagent grâce à l'ionosphère, une couche atmosphérique dont les perturbations dues à l'activité géomagnétique causent l'évanouissement et le décalage Doppler du signal. Ces effets Doppler peuvent être très intenses dans les régions polaires et aurorales et affecter ainsi la fiabilité et la constance des liens de communications. La dispersion temporelle crée un étalement causé par les trajets multiples pour chaque mode et on peut observer plusieurs modes produits par la réflexion sur différentes couches ionosphériques ou des trajets comportant plusieurs réflexions, notamment sur la Terre. Les paramètres de propagation sont donc plutôt dynamiques et on observe des tendances diurnes, saisonnières ou pendant le cycle solaire pluriannuel, et selon la fréquence utilisée. Pour concevoir et évaluer les technologies radio adaptées à ces conditions, il sera nécessaire de caractériser les paramètres de propagation pour un éventail de liens de communication à différents moments. Les campagnes de mesure visant à déterminer les différentes gammes de paramètres exigent des sondeurs de canaux conçus avec soin. Des séquences de pseudo bruit ayant des caractéristiques de compressions d'impulsions sont adéquates pour extraire les réponses des canaux tout en exigeant peu de traitement de signal. Le présent article contient notre évaluation des différentes séquences périodiques et apériodiques de pseudo bruit, pour un vaste éventail de conditions de propagation obtenues lors de campagnes antérieures de sondage à haute altitude. Nous avons

trouvé que les séquences apériodiques courtes sont le choix le plus fiable : bien qu'elles présentent peu d'avantages en matière de traitement, elles sont suffisamment courtes pour limiter les distorsions causées par l'évanouissement et le décalage Doppler, et on peut ajuster leur utilisation pour obtenir des compromis permettant de mesurer la gamme désirée de trajets multiples et d'étalement Doppler. D'autres composants de la forme d'onde de sondage pourraient inclure la capacité de résoudre les ambiguïtés des retards et de fréquences.

# Table of contents

# List of figures

# 1 Introduction

HF is still used as an alternative to satellite bearers for beyond-line-of-sight (BLOS) communication in the Canadian Armed Forces (CAF) [1]. When satellite communication is not available due to lack of coverage, jamming or congestion, HF radios are needed to support strategic and tactical operational command and control.

HF radios operate in the range 3-30 MHz, and for BLOS, or skywave, communication, the signals propagate by reflection from the ionosphere, which is an atmospheric layer of increased electron density approximately 75-1000 km above the Earth [2]. Irregularities in the electron density cause scattering of the signal, which results in scintillation [3]. Many different component waves combine in the received signal, which results in spectral broadening or Doppler spread, and causes fading. The received signal is spread in time due to the reflective and refractive process through the ionosphere, and mass movement of the electron density regions, particularly in the polar regions, causes a frequency offset, or Doppler shift, in the received signal.

These severe disturbances are primarily observed in high-latitude (polar and auroral) and equatorial regions, and are associated with geomagnetic storm activity [4], as well as diurnal solar effects [5]. Lower layer ionisation causes absorption, or attenuation of the radio signals, particularly during daytime. In the auroral region, the degree of absorption can vary rapidly in time and space [6].

The electron density profile of the ionosphere varies diurnally and seasonally, and by the sunspot activity. Sunspots are associated with strong magnetic fields, which increase the level and variation of ionisation. There is a multi-year variation in the number of sunspots, with cycles of between 7 and 15 years, typically averaging around 11 years [2]. The HF propagation characteristics therefore vary over many years [6].

HF radio signals emitted from the Earth's surface will be reflected by one or more regions of the ionosphere, depending on their frequency, incidence angle, and the electron density. Signals may also be reflected from the Earth's surface, resulting in multi-hop propagation, and enabling communications over extremely long distances – signals have been observed traversing the long great circle path from Norway to Ottawa, via the southern hemisphere, a distance of over 33 000 km. Signals arriving at the receiver may therefore have several modes, each having travelled over different paths, with different altitudes, experiencing different conditions that affect delay, attenuation, Doppler shift and spread.

The propagation conditions experienced by an HF radio system therefore depend on location, frequency, time-of-day, season, and geomagnetic and solar activity, and the range of conditions is particularly extreme and dynamic at high latitudes, i.e., in polar and auroral regions.

Measurements comparing mid- and high-latitude conditions show a distinct difference in propagation parameters, particularly in their variation [7]. However, it should be noted that extreme HF propagation can be observed in other regions, for example during darkness in the mid-latitude trough [8], which is a region of the ionosphere where electron density is depleted at night [9]. Measurements in the equatorial region showed higher Doppler spreads during daylight, and more consistency from day to day compared to high latitudes [10].

To specify the operating requirements for HF radios, it is necessary to have a good understanding of the range of conditions that may be observed. To adequately test HF radios, they must be exposed to this full range of conditions. To compare HF radios, their performance over known conditions within this range should be evaluated.

For over-the-air testing, identifying the range of conditions the radio system is exposed to is a challenge, as radios do not typically parameterise the channels they use. One option is to operate a channel sounder on an adjacent frequency channel, so that performance and propagation conditions can be correlated. However, this does not ensure that the radios are being tested over the full range of conditions that it is required to support, and very extensive testing in a range of locations, times of day and seasons may be required.

For efficacious design and evaluation of HF radio technology, characterisation and modelling of HF channels under a wide range of conditions is essential. This facilitates channel emulation or simulation, whereby the channel conditions can be controlled and reproduced for offline testing and comparison of radio technologies [11]. Measurement of HF channels is achieved by channel sounding, in which specially designed signals, or probes, are used to extract specific propagation parameters.

HF channel sounding for scientific exploration and technology development has been of interest for many decades. Chirp sounders have been used since the 1920s to estimate the height at which HF signals are reflected. These became known as ionosondes, and by the 1950s and 1960s, their swept frequency chirps are still producing detailed ionograms, i.e., profiles of time-of-flight (indicative of reflection height) vs. frequency delay at locations across the globe, e.g., [12]. The Canadian Advanced Digital Ionosonde (CADI) is operated by the University of New Brunswick as part of the Canadian High Arctic Ionospheric Network (CHAIN) [13], and provides detailed measurements for the purpose of understanding the sources and dynamic characteristics of ionospheric properties in the polar cap and auroral zones. An extensive list of active ionosondes is found at [14], including several in Greenland, Norway, Russia and Alaska and in Antarctica.

In the 1960s, the Canadian Defence Research Telecommunications Establishment (DRTE), which later became the Communications Research Centre, developed an ionospheric sounder based on pulse compression sequences to avoid the high peak-to-average power requirements of a pulse sounder [15]. This concept was adopted in the early 1980s by the US Naval Research Laboratory (NRL), which developed a wideband HF sounder to measure the extended line-of-sight (ELOS) surface wave channel [16]. The sounder operated at bandwidths up to wideband 1 MHz, and was used to obtain high resolution observations of a long trans-auroral path, showing delay spreads up to 1 ms and Doppler spreads in the range 5-10 Hz [17]. In the 1990s, the DAMSON (Doppler And Multipath SOunding Network) [18] was built and installed at locations in northern Europe and characterised BLOS paths in the auroral, sub-auroral and polar regions for more than half a solar cycle in the mid- to late-1990s. Results from these multi-year measurements showed that that the characteristics observed in [17] were far from extreme [19–21].

Both the NRL sounder and DAMSON used pseudo-noise sequences to probe the channel and estimate its response. This approach has been widely used across a range of frequencies and environments [22–27]. While the chirp channel probe sounder used in [28] swept each HF channel quite rapidly, the rate was too slow to tolerate the very high Doppler spreads that may be observed at in polar regions. With the pseudo-noise probes, the probing sequence can be selected to support a channel response rate that accommodates the extreme characteristics expected in these regions. In both cases, the channel responses may be combined to form a delay-Doppler scattering function [29, 30], or spectrogram, which supports the investigation of the almost-instantaneous delay and Doppler characteristics of the propagating modes.

In the early 2000s, Australia's Defence Science and Technology Group undertook an HF channel characterisation campaign in mid- and equatorial latitudes using a chirp-type sounder. This was able to extract various propagation parameters including the time-of-flight, attenuation and delay-Doppler scattering function [28].

Modern HF radios may operate over wider bandwidths than the conventional 3 kHz channel assignments that were used in the original DAMSON sounder [31]. For example, the most recent revisions of the US HF radio standards (Mil-Std-188-141C and Mil-Std-188-110C) include waveforms for wideband HF (WBHF) over channels of up to 24 kHz bandwith. Alternatively, data rates may be increased by aggregating non-contiguous narrowband channels [32, 33]. New sounding campaigns and enhanced HF channel models are required to support advances in HF communication technology.

This purpose of this report is to review the channel sounding methodology, to summarise the considerations necessary in designing a suitable sounding waveform, and to make recommendations about waveform selection for high-latitude HF measurements. The report is written in support of the work of the Technical Cooperation Program (TTCP) Command, Control, Communications, Cyber and Information (C4I) Group's Technical Panel on Communications in the area of high-latitude BLOS communications. It draws on the work and results of the DAMSON project, supplemented by experience from channel measurement, characterisation and modelling campaigns in other frequency bands and environments.

In the next section, an overview of the DAMSON project is given, and the range of channel conditions observed is summarised. Experience with this sounder indicates that the pseudo-noise probing sequence approach is well-suited to the propagation conditions expected at high-latitudes, and this will be the approach considered herein. The principles for obtaining channel responses using pseudo-noise sequences are outlined in Section 3, and candidate probing sequences are presented and evaluated in Section 4. Based on this analysis, recommendations for designing sounding waveforms are made in Section 6. Concluding remarks are made in Section 7.

# 2 The DAMSON project

The DAMSON project (Doppler And Multipath SOunding Network) [10] was a collaboration of the UK's Defence Evaluation Research Agency (DERA), Norway's Forsvarets Forskningsinstitutt (FFI), Sweden's Försvarets Forskningsanstalt (FOA) and Canada's Communications Research Centre (CRC). The project was originally formulated around 1994, and the system operated from the mid-1990's to the early 2000's, through more than half a solar cycle. The system was installed with two transmitters and two receivers in northern Scandinavia, cycling through 10 frequencies continuously to characterise all four paths.

The original DAMSON system operated on conventional 3 kHz HF channels, although it was upgraded to 12 kHz channels late in its life: this warranted a minor redesign of its sounding waveform, but the core features remained the same. The key parameters extracted from the channel sounding were the number of modes, and for each, the signal-to-noise ratio (SNR), Doppler spread, Doppler shift and delay spread. Using the values obtained from measurements, the widely-used tapped-delay line Watterson HF channel model [34], could be parameterised; further, the time-varying nature of those key parameters could be modelled.

The channel characterisations obtained with the DAMSON system were used to define the requirements for the NATO robust HF waveform, STANAG 4415 [35], which is also included in the US Mil-Std 188-110A/B/C standards as well as in NATO STANAG 4539 [36], and also supported the development of the HF automatic radio control system standard, STANAG 4538 [37].

## 2.1 Sounder design

In its normal operation, the 3 kHz DAMSON channel sounder dwelled for intervals of one minute on each of ten prescribed frequencies, cycling repeatedly through the set. The transmitter and receiver have GPS receivers, to synchronise in both time and frequency. Within each interval was a delay-Doppler (DD) mode, a continuous wave (CW) mode, a time-of-flight (TOF) mode and a passive sensing period for noise measurement (NM). The DD mode is the part of the waveform of most interest for extracting the propagation characteristics, and will be addressed in detail below.

An example of the output produced by the DAMSON sounder is shown in Figure 1. This is taken from the Svalbard-to-Tuentangen link at 4.7 MHz in September 1995. The central panel shows the delay-Doppler (DD) spectrogram, which was generated as described in Section 3.2, using channel response estimates obtained using a pseudo-noise probing signal (Section 3.1). This mode lasted only 1.6 s, but from the output, the modes were identified and their SNRs, delay spreads and Doppler parameters were extracted. This example shows a single propagating mode with negligible Doppler shift, a Doppler spread of approximately 20 Hz and a modal delay of around 8 ms. As the DAMSON project proceeded, the process of identifying and parameterising modes became more and more automated, but manual oversight was always required to deal with ambiguous or anomalous cases.

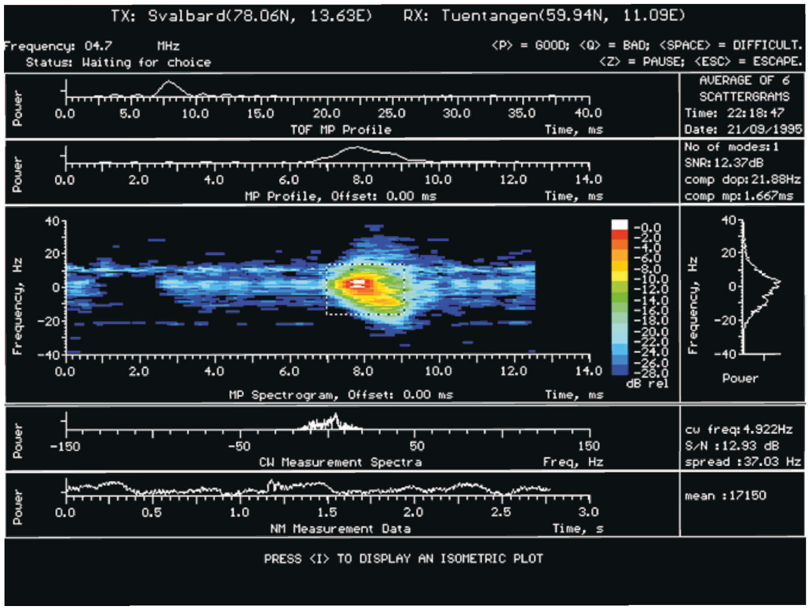


***Figure 1:*** *Example DAMSON output, from [38].*

The top panel in Figure 1 shows the time-of-flight (TOF) profile, which used the same pseudo-noise sequence as in the DD mode, but transmitted less frequently, providing a resolution of modal times-of-flight up to 40 ms. This provided a way to determine whether the signals observed took the shortest route from transmitter to receiver, or were propagated the long way around the earth, which was seen not infrequently, especially when testing at lower latitudes.

The delay-Doppler spectrogram has its time domain contour (the multipath profile) above, and its frequency domain contour to the right; these assisted in interpreting the SNR colours of the spectrogram. Below the spectrogram is the CW output, which was derived by transmitting a single tone over an interval of approximately 4 s. This provided an accurate indication of whether there was support for ionospheric communications – a signal might be seen here when the SNR was insufficient to extract detailed propagation characteristics, and also allowed for the unambiguous Doppler resolution of the modes.

Finally, the received signal power during the passive NM mode is shown in the bottom panel, which allowed other background interferers to be identified; other users were often observed on the same assigned channel given the long range of HF communications and the propagation of signals beyond national regulatory boundaries. Often, Morse code, which was still widely used by maritimers during the DAMSON period of operation, would be observed in this interval.

## 2.2 Summary of DAMSON results

DAMSON transmitters and receivers were located in northern Europe to measure the channel characteristics of BLOS paths in the auroral, sub-auroral and polar regions. Multi-year (24 hr/day) measurements were obtained using transmitters at Isfjord on Svalbard (78.06N, 13.63 E), and Harstad, Norway (68.06N, 16.03E) and receivers at Tuentangen, Norway (59.94N, 11.09E) and Kiruna, Sweden (67.84N, 20.40E). See Figure 2, which also shows the approximated auroral region for midnight when the planetary average geomagnetic index is $Kp = 5$, indicating a minor storm. Soundings were made every 10 minutes on each of 10 frequencies from 2.8 MHz to 21.9 MHz. The summary here is obtained mainly from the analysis of data from spring and fall 1995 [39], which was used to support the selection of parameters used in the selection and specification of the NATO Robust Waveform [35]. Additional analysis of these data sets was presented in [38].

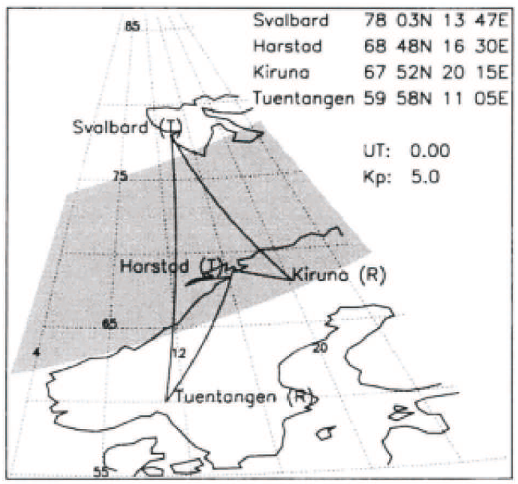


***Figure 2:*** *Locations of DAMSON transmitters and receivers, and auroral region for midnight during high geomagnetic activity, from [38].*

The three longest links are more-or-less oriented north-to-south, and long enough that prediction programs indicate multihop propagation as well as multiple modes for some frequencies and times-of-day. One is generally sub-auroral, except during highly geomagnetically active periods; the multi-hop paths on the longest may reflect from ionospheric regions inside the polar cap, in the auroral zone or below the auroral zone; and the most northerly path lies almost completely in the auroral region, ensuring that reflection zones are in a highly disturbed region of the ionosphere.

The Doppler spreads and multipath spreads on these three links vary in accordance with the level of disturbance in their reflection zones. On the sub-auroral Harstad-Tuentangen link, the mean Doppler spreads were low, $< 2$ Hz, across the range of frequencies and time, but tended to be more varied at night, with 95th percentiles up to 6 Hz. Doppler shifts remained within $\pm 2.5$ Hz, and the mean tended negative with increasing frequency, to approximately -0.5 Hz at 22 MHz. Multimodal propagation was common, particularly at the lower frequency range ($< 8$ MHz), and the overall multipath spreads were concomitantly higher, with 95th percentiles up to 5 ms during daylight, and 6 ms in darkness. Similar multipath spreads were observed on the long Isfjord-Tuentangen link, where multiple modes were seen often at lower frequencies. At higher frequencies, single propagating modes were usual, with mean multipath spreads near the lower limit of the DAMSON resolution, approximately 0.6 ms. The higher latitude reflection regions, however, resulted in much higher Doppler spreads, with 95th percentiles reaching 15 Hz during darkness, with some daytime observations reaching this range. Upper limits on observed Doppler shift were in the range of $\pm 5$ Hz, and as on the Harstad-Tuentangen link, the trend was for negative mean Doppler shifts at higher frequencies.

The 1150 km Isfjord-Kiruna path lies almost completely in the auroral region, ensuring that reflection zones are in a highly disturbed region of the ionosphere. The impact of the more northerly reflection zones was evident in the measurements of Doppler spread, with 95th percentiles exceeding 40 Hz at some frequencies. The mean Doppler spreads were larger than 3 Hz, and sometimes exceeded 10 Hz. Doppler shifts were also high, with 95th percentiles exceeding $\pm 15$ Hz, and even reaching $\pm 40$ Hz for some periods. Multipath spreads were also high, with 95th percentiles approaching 9 ms for some frequencies, arising due to the large number of propagating modes (means of approximately 2.5 modes during some periods).

The short (180 km) link, almost west-to-east, from Harstad to Kiruna is considered a near-vertical incident skywave (NVIS) path, which means that the elevation angles are high at the transmitter and receiver and only the lower HF frequency range will propagate – this range has higher absorption, so communication over NVIS paths needs to be able operate at low SNR, or requires higher transmitter power. The NVIS range is up to approximately 200 km [40], so there may be some groundwave signal propagating, which causes self-interference at the receiver. The DAMSON system was used to characterise NVIS links, both on the 180 km Harstad-Kiruna link, and from Harstad-Abisko (68.34N 18.83E), which is a 120 km link, as reported in [41]. For the Harstad-Kiruna link, in the mid-frequency range, multipath spreads were observed at the limit of the DAMSON system, i.e., 12.5 ms, with more than five propagating modes. Large Doppler spreads were also observed, particularly in darkness, with 90th percentiles greater than 60 Hz, and Doppler shifts exceeding $\pm 20$ Hz were not uncommon.

As noted, across much of the frequency range, and over much of the diurnal cycle, multiple modes propagate. In parameterising models, it is necessary to apportion power appropriately amongst the modes. It was reported in [42] that an even distribution of power amongst the modes was unsuitable in over one-third of bi-modal observations; further, it was observed that the first mode (shortest time-of-flight) is often not the strongest.

The second-order characteristics of these channels should also be modelled. Analysis reported in [21, 43] showed that the parameters change rapidly, with wide variations over short periods of time, such as tens of minutes. This may impact the adaptivity response required in an HF radio system.

Over the several years of the DAMSON project, it became evident that HF propagation observed on high latitude BLOS channels indicates that HF radios must be able to support multiple modes with delay spreads up to at least 12.5 ms, Doppler spreads in excess of 50 Hz and Doppler shifts up to 30 Hz.

# 3 Channel sounding

As described in Section 2, there are several potential components to a composite HF sounding waveform that supports resolution of ambiguities in time and frequency. At the core of the DAMSON sounder is the estimation of channel impulse responses, as with other channel sounders, e.g., mobile channels across the UHF band [22, 26, 27, 44]. The most commonly used, relatively easy to implement, approach is to use a pseudo-noise probing sequence. The signal processing underlying this approach is summarised in Section 3.1, and the processing to generate a delay-Doppler scattering function for the estimation of channel parameters is described in Section 3.2. In rapidly time-varying channels, such as might be expected at high-latitudes, the channel distortion impacts the accuracy with which the channel response can be estimated, and the selection of an appropriate sequence requires some trade-offs. The suitability of several possible probing sequences is considered in Section 4, and some comments on the use of the coherence time concept are given in Section 5.

## 3.1 Channel estimation

Although standard 3 kHz and 12 kHz HF communications are frequently described as narrowband, from a propagation perspective the channels would be defined as wideband, or frequency selective, as their delay spreads exceed a single symbol interval, at least in multi-modal cases. The Watterson HF channel model [34] defaults to a narrowband (flat fading) channel when there is only a single propagating mode, but this model is known to be limited, in particular in that it does not model "spread-F", which is time dispersion within the F-layer of the ionosphere [6], i.e., above about 140 km altitude. In addition, the Watterson model was derived (using only a short measurement campaign over a single path in a mid-latitude region) for 3 kHz channels; as wider bandwidth radios are considered for more robust and higher rate communications [31], the time dispersion on individual modes will become more relevant.

The complex channel response is dependent on time, and can be written $h(t,\tau)$, describing the response at time $t$ to an impulse transmitted at $t-\tau$, The signal received when the transmitted signal is $s(t)$ is then given by

$$r(t) = \int_0^{\tau_{max}} h(t,\tau)s(t-\tau)d\tau + \eta(t) \tag{1}$$

where $\eta(t)$ is additive white noise, with zero mean and variance $\sigma_\eta^2$. The integral is bounded by the maximum multipath delay, $\tau_{max}$.

It is usual to consider a sampled model, with taps spaced by intervals $\Delta t$, in which case (1) is written

$$r(n) = \sum_{\ell=0}^{L_{max}} h(n,\ell)s(n-\ell) + \eta(n) \tag{2}$$

where $h(n,\ell)$ is the complex response to an impulse transmitted at time interval $n-\ell$. The $L_{max}+1$ terms of $h(n,\ell)$ then give the tap gains on a tapped-delay line channel model.

Generating a reasonable facsimile of an impulse is challenging, and requires a high peak-to-average transmitted power ratio to obtain a sufficient signal-to-noise ratio (SNR) at the receiver for a good quality estimate. The use of pulse compression probing signals alleviates this problem, as there is a range of sequences that have autocorrelation functions (ACFs) closely approximating an impulse. For a sequence $s(1)\ldots s(K')$, the ACF is defined as

$$\phi_{ss}(m) = \sum_{k=1}^{K'} s(k)s^*(k+m) \tag{3}$$

where $^*$ denotes the complex conjugate. The aim when selecting a probing sequence is then to choose one such that

$$\phi_{ss}(m) = \sum_{k=1}^{K'} |s(k)|^2 \qquad m = 0 \tag{4a}$$

$$\approx \qquad 0 \qquad m \neq 0. \tag{4b}$$

The sequence may be aperiodic or periodic; for the former, the pseudo-noise sequence is length $K \leq (K'+1)/2$, and is followed by at least $(K-1)$ null symbols. Periodic sequences are of length $K = K'$, i.e., $s(k) \neq 0$ for all $k = 1,\ldots,K'$, and the sequence repeats continuously. In either case, if the sequence has a uniform unit envelope, i.e., $|s(k)|^2 = 1$ for $k = 1,\ldots,K$, the peak at $m = 0$ is $K$.

Correlating the sampled received signal $r$ in (2) with the complex conjugate of the probing sequence gives the received correlation function (RCF)

$$\phi_{rs}(-m) = \sum_{n=m+1}^{m+K} r(n)s^*(n-m) \tag{6a}$$

$$= \sum_{\ell=0}^{L_{max}} \sum_{n=m+1}^{m+K} h(n,\ell)s(n-\ell)s^*(n-m) + \sum_{n=m+1}^{m+K} \eta(n)s^*(n-m) \tag{6b}$$

where the final term can be written as additive noise $\nu(m)$, with mean zero and variance $\sigma_\eta^2 \sum_{k=1}^{K} |s(k)|^2$.

Assume, for now, that channel response $h(n,\ell)$ remains constant over the length of the probing sequence. Then, replacing $j = n-m$ in the summation yields

$$\phi_{rs}(-m) = \sum_{\ell=0}^{L_{max}} h(n,\ell) \sum_{j=1}^{K} s^*(j)s(j+m-\ell) + \nu(m) \tag{8a}$$

$$= \sum_{\ell=0}^{L_{max}} h(n,\ell)\phi_{ss}^*(m-\ell) + \nu(m). \tag{8b}$$

Now, assuming an ideal probing signal as in (4a) and (4b), for which the correlation results in a delta function, the RCF becomes

$$\phi_{rs}(-m) = Kh(n,m) + \nu(m). \tag{10}$$

Thus, for a unit envelope probing sequence, the channel impulse response estimate at time interval $n$ is given by $\hat{h}(n,\ell) = \frac{1}{K}\phi_{rs}(-\ell)$.

As noted above, this formulation applies to periodic and aperiodic probe sequences, as long as the latter are interspersed with null intervals of at least $K-1$ symbols.

## 3.2 Delay-Doppler scattering function

The channel estimation process is used over multiple sequential sequence lengths to provide a series of channel estimates $\hat{h}(n,\ell)$. The delay-Doppler spreading function, first introduced by Bello [45], and also known as the delay-Doppler scattering function in [29] or the spectrogram in the DAMSON literature, provides a mechanism to visualise the characteristics of the channel, as was illustrated in Figure 1.

For the continuous time model, (1), $h(t,\tau)$ is called, in the terminology of Bello [45] and subsequent authors, the "input delay-spread function". This can be written as

$$h(t,\tau) = \int H(f,\tau)e^{j2\pi ft}df \tag{11}$$

i.e., as the inverse Fourier transform of its delay-Doppler scattering function, $H(f,\tau)$, which describes the frequency response of the channel at a delay $\tau$.

For the series of $N$ channel impulse response estimates $\hat{h}(n,\ell)$ obtained in Section 3.1, the delay-Doppler scattering function describes the Doppler spectrum at each delay $\ell$, i.e.,

$$H(\omega,\ell) = \sum_{n=0}^{N-1} \hat{h}(n,\ell)e^{-j\frac{2\pi}{N}n\omega} \qquad \omega = 0,\ldots,N-1 \tag{12}$$

sampled in frequency $\omega$ at intervals $\Delta f = 1/NT$ Hz, where $T$ is the interval between consecutive channel impulse response estimates. For a baud rate of $B$, the probing sequence repeats at intervals $T = K'/B$.

The range of the delay-Doppler scattering function is determined by the signal baud rate, $B$, and the parameters of the probing signal. The delay resolution is $1/B$, for ideal filtering, and the maximum multipath spread that can be accommodated is $T = K'/B$ s. For a sequence of total length $T$ s repeated $N$ times, the integration time is $NT$ s, and the frequency resolution is $1/NT = B/NK'$ Hz. The maximum width of a Doppler spectrum that will not be aliased is $1/T$. The processing gain is $10\log_{10}\sum_{k=1}^{K'}|s(k)|^2$, which is $10\log_{10}K$ for a unit envelope pseudo-noise sequence of length $K$.

An example of the absolute scattering function, or spectrogram, from the DAMSON system was shown in Figure 1. Within it, the propagating modes are quite clearly defined, and the Doppler and multipath spreads can be extracted for each mode. In the DAMSON system, these parameters were computed by finding the limits that contained 95% of the modal powers. Within this time-frequency box, the delay and Doppler spreads were computed as the two-sided standard deviation ($2\sigma$) values, per the usual definition, based on an assumption of Gaussian distributions.

The generation of the delay-Doppler scattering function requires an assumption of WSSUS. This means the statistics of each channel tap are assumed to be wide-sense stationary (WSS), i.e., they have constant mean and autocorrelation [46], over the interval used to compute the delay-Doppler scattering function. Further, different path delays or taps are assumed to have uncorrelated scattering (US). This latter assumption may be violated in the channel estimation process, depending on the receiver filter characteristics; in the DAMSON system this was alleviated by estimating the Doppler spread across the whole mode, rather than at individual delays. This is consistent with the Watterson HF channel model [34], in which each mode is assigned a single tap in the tapped delay line model. For wider bandwidth sounders, with a better time resolution, some care in filter design and data analysis would be required to evaluate the validity of this assumption.

In general, the WSSUS assumption can be taken as valid as long as the duration of the measurement is sufficiently short. Due to the lack of measurement data, a definition of "sufficiently" is not easily prescribed, analysis of the DAMSON data [21, 43], described in Section 2.2 showed that Doppler spread estimates remained within ±1 Hz for at least 10 minutes, on average, on all the sub-auroral and trans-auroral paths measured, which is far longer than a delay-Doppler measurement would last in practice.

# 4 Sequence selection

In this section, several pseudo-noise sequences with good autocorrelation functions are evaluated for use as sounder probing sequences. Both aperiodic sequences, i.e., requiring null intervals, and periodic sequences, i.e., transmitted contiguously, are considered; the former were used in the DAMSON system and the latter are widely used in characterising mobile UHF channels. Two metrics are considered, the peak-to-maximum-sidelobe ratio and the merit factor; others have been used in evaluating sequences, but have not been found to be as easily interpreted or as discriminatory.

## 4.1 Sequences considered

As noted above, sounding sequences might be aperiodic, i.e., sequences of length $K$ with at least $K-1$ nulls between instances, or periodic, i.e., sequence follows sequence with no space between. Several sequences of each type have been evaluated, as described below. Recall that the baud rate is $B$, the sequence is non-zero over $K$ adjacent symbol intervals of length $1/B$, and repeats every $K'$ intervals, or $T = K'/B$ s.

### 4.1.1 Aperiodic sequences

The advantage of aperiodic sequences is that, subject to the minimum length of the space of $K-1$ symbol intervals, the sequences can be separated as much as desired. This allows flexibility of design to balance the maximum measurable multipath spread and Doppler spread.

The sequences considered here were (the codes are defined in Annex A):

**Barker 13** a binary sequence, transmitted using binary phase shift keying (BPSK), or $+1$ and $-1$. It is the longest of the real-valued Barker sequences [47], and is a pulse compression sequence, i.e., the arrangement of its bits are similar to a chirp. The ACFs of Barker sequences have maximum sidelobes of amplitude 1.

**Barker 25** a complex sequence with a uniform envelope, which is specified by the phase values for each symbol [48]. It has a maximum ACF sidelobe of amplitude 1.

**Somaini** complex sequences with uniform envelopes, and maximum ACF sidelobe of amplitude 1 [49]. Somaini sequences lengths $K = 13$, 25 and 64 are considered.

**Huffman** real non-uniform sequences, with symbol amplitudes varying from less than 1 to over 65, taking positive and negative values. The ACF of this sequence is perfect, i.e., the maximum sidelobe is zero. The Huffman sequences are constructed per [50], with lengths $K = 35$ and $K = 51$. The maximum amplitude of the Huffman 35 is approximately 65, and for the Huffman 51, it is 695.

**FZC** uniform complex Frank-Zadoff-Chu sequence swith perfect ACF. The FZC sequences are constructed as in [51], with lengths $K = 30$ and $K = 60$.

### 4.1.2 Periodic sequences

Using periodic sequences means that energy is transmitted in every symbol interval during the probing period, which means that the received signal-to-noise ratio is maximised for each channel response measurement. Periodic sequences, in particular the binary maximal-length sequence, or m-sequence, are widely used in channel sounding for a range of other time-varying channels at VHF and above, including urban vehicular [22–24], space-time in a variety of environments [25, 26], and air-to-ground [27].

Real-valued m-sequences are available with lengths $2^n - 1$ for integer $n$. They are binary sequences, generated using a feedback shift generator and transmitted using BPSK. The ACFs for m-sequence have uniform sidelobes of $-1$. Sequence lengths of 7, 15, 31 and 63, generated using shift registers of length $n = 3, 4, 5$ and 6, were considered here. The shift register implementation for m-sequence 7 is shown in Figure 3, the shift register taps are given in Annex A.3.

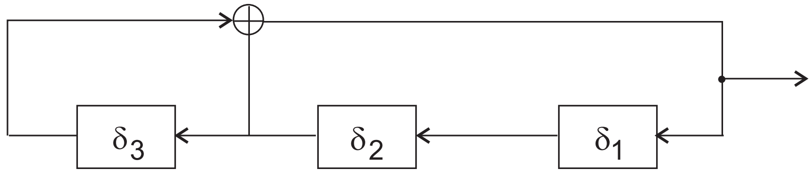


***Figure 3:*** *Shift register configuration for m-sequence 7.*

## 4.2 Metrics

Several metrics have been proposed for evaluating sequence properties, and were considered for selecting a DAMSON sequence for the 12 kHz system. These include energy efficiency, i.e., the amount of energy contained in the peak $\phi_{rs}(0)$ vs. the sidelobes, and the position of the maximum sidelobe, i.e., the value of $m \neq 0$ with the largest value $|\phi_{rs}(m)|$. However,it was found during the DAMSON analysis that they were not particularly helpful in discriminating amongst the sequences when considering the impacts of channel distortions such as Doppler spread and shift.

As seen above, the length of the sequence as well as its cross-correlation properties, are key to a good selection. The delay, Doppler shift and spread conditions expected on the channel will determine the degree of distorting effects, with shorter sequences being less affected. However, longer sequences give better processing gains, which enables weaker modes to be observed and characterised, so these two factors must be balanced.

The length of the sequence determines the processing gain, i.e., the the signal-to-noise ratio (SNR) enhancement at the processor output, given (in dB) by

$$PG = 10 \log_{10} \sum_{k=1}^{K'} |s(k)|^2. \tag{13}$$

The length of the sequence also determines the minimum repetition interval $T = K'/B$ where $B$ is the baud rate: for aperiodic sequences of length $K$, the minimum repetition interval is $K' = 2K - 1$ intervals; for periodic sequences, the sequence must continuously repeat, hence $T = K/B$.

The sequence repetition interval $T$ must be long enough that the propagation modes can be clearly seen, i.e., $T$ must exceed $\tau_{max}$, the delay spread of the channel, but this parameter also limits the range of Doppler spreads that can be distinguished in the delay-Doppler spectrogram, Sec. 3.2. If the Doppler power spectrum exceeds the breadth of the spectrogram, i.e., $1/T$, then it will be aliased and the parameters will be unresolvable. Using the Gaussian power spectrum to model the Doppler fading (17), it is seen that if $\frac{1}{2T} > 2\sigma_h$, then the Doppler power spectrum would be at less than 15% of its peak at the edge of the spectrogram, which will have a relatively small aliasing effect.

In addition to the length of the sequence, the structure of the sequence also affects the impact of Doppler spread and shift. To assess this impact, the two most useful metrics were found to be the peak-to-maximum sidelobe ratio (PMR) [47]

$$PMR = \frac{\phi_{rs}(0)}{\max_{m,m\neq 0} \phi_{rs}(m)} \tag{14}$$

and the merit factor (MF) [51]

$$MF = \frac{[\phi_{rs}(0)]^2}{2\sum_{m=1}^{M} [\phi_{rs}(m)]^2}. \tag{15}$$

The PMR is important, because it determines when a propagation mode can be distinguished clearly from artifices created by the receiver processing. When sidelobes are too large, they may obscure, or be misinterpreted as, propagating modes with different Doppler shifts. The MF provides a more general metric to assess how well the correlation peak can be discriminated amongst all the sidelobes.

## 4.3 Sequence evaluation

Per the DAMSON observations, Sec. 2.2, a high-latitude HF sounder for measuring channel characteristics in polar, auroral an sub-auroral regions should be capable of capturing Doppler spreads in excess of 50 Hz, multipath spreads up to at least 12 ms. To generate a Doppler power spectrum achieving these ranges, channel response estimates are needed at intervals satisfying $T \ll 1/50 = 20\ ms$. Thus, a channel response estimate of length $T = 12$ to 15 ms, with corresponding Doppler ranges ±42 to ±33 would be ideal.

For a baud rate of 2400 samp/s, as typically used in a 3 kHz channel, this channel response length corresponds to 29–36 samples. For a 12 kHz channel, with baud rate 9600 samp/s, longer sequences of 116–144 samples could be used.

Note that a measurement system must also be capable of measuring Doppler shifts up to ±40 Hz. The Doppler power spectrum does not allow the resolution of Doppler shifts, as those exceeding $\pm\frac{1}{2T}$ will alias into this range. Resolving Doppler shifts would require, as in the DAMSON case, a period of continuous wave transmission.

## 4.4 Aperiodic sequences

The characteristics of the aperiodic sequences are summarised in Table 1, where the ‘ideal’ characteristics refer to the case of an undistorted channel. Plots of the PMR and MF for unimodal Gaussian fading with Doppler spreads up to 50 Hz and Doppler shifts up to 30 Hz are shown in Figures 4 and 5 for baud rate $B = 2400$, respectively, in Figures 6 and 7 for $B = 9600$ and in Figures 8 and 9 for $B = 24k$.

***Table 1:*** *General ACF characteristics of aperiodic sequences.*

| sequence | ideal PMR | ideal MF | PG (dB) |
|---|---|---|---|
| Barker 13 | 13 | 14.1 | 11.1 |
| Somaini 13 | 13 | 17.5 | 11.1 |
| Barker 25 | 25 | 16.6 | 14.0 |
| Somaini 25 | 25 | 22.5 | 14.0 |
| FZC 30 | 30 | 8.5 | 14.8 |
| Huffman 35 | 35 | $\infty$ | 15.4 |
| Huffman 51 | 51 | $\infty$ | 17.1 |
| FZC 60 | 60 | 12.4 | 17.8 |
| Somaini 64 | 64 | 35 | 18.1 |

***Table 2:*** *General delay-Doppler characteristics of aperiodic sequences.*

| sequence | minimum $T$ (ms) | | | maximum Doppler spread (Hz) | | |
|---|---|---|---|---|---|---|
| | $B = 2400$ | $B = 9600$ | $B = 24k$ | $B = 2400$ | $B = 9600$ | $B = 24k$ |
| Barker 13 | 10.4 | 2.6 | 1.0 | 48.0 | 192.0 | 480.0 |
| Somaini 13 | 10.4 | 2.6 | 1.0 | 48.0 | 192.0 | 480.0 |
| Barker 25 | 20.4 | 5.1 | 2.0 | 24.5 | 98.0 | 244.9 |
| Somaini 25 | 20.4 | 5.1 | 2.0 | 24.5 | 98.0 | 244.9 |
| FZC 30 | 24.6 | 6.1 | 2.5 | 20.3 | 81.4 | 203.4 |
| Huffman 35 | 28.8 | 7.2 | 2.9 | 17.4 | 69.6 | 173.9 |
| Huffman 51 | 42.1 | 10.5 | 4.2 | 11.9 | 47.5 | 118.8 |
| FZC 60 | 49.6 | 12.4 | 5.0 | 10.1 | 40.3 | 100.8 |
| Somaini 64 | 52.9 | 13.2 | 5.3 | 9.4 | 37.8 | 94.5 |

It is clear from these results that the Huffman sequences have the best performance, maintaining high values of PMR and MF over the range of distortions considered. However, note from Table 2, which shows the minimum delay range and corresponding maximum Doppler spread ranges for each aperiodic sequence, that these sequences are too long to support sufficient Doppler spread range at $B = 2400$. In addition, the transmitted peak-to-average powers of the Huffman 35 and 51 sequences are 40 dB and 60 dB, respectively, which makes them unsuitable in most cases even at higher baud rates.

The longest sequences, FZC 60 and Somaini 64, both have sufficient delay ranges, and marginally deficient Doppler ranges, at 9600 baud. However, the length is a disadvantage when it comes to tolerating distortions, in particular Doppler spread, with PMR near or below one for combinations of high Doppler shift and Doppler spread.

The length-25 sequences, Barker 25 and Somaini 25, are too long for use at $B = 2400$, but at $B = 9600$ and higher, they sustain their PMR and MF well over the desired range of Doppler spread and shift.

The shortest sequences considered, Barker 13 and Somaini 13, perform the best of the uniform envelope sequences in terms of PMR and MF at high values of Doppler shift and spread. For small distortions, the effect of the small processing gain is seen in both metrics at very low values of Doppler shift and spread, but this is rapidly overcome for shifts of approximately 2 Hz at $B = 2400$, and 10 Hz at $B = 9600$, or for spreads above about 5 Hz and 35 Hz for the two baud rates. Both the length 13 and 25 pairs of sequences perform well at $B = 24k$, but the short ones are more consistent, and more tolerant to high levels of both Doppler shift and spread.

There is a slight advantage for the complex-valued sequence, Somaini 13, over the real-valued Barker 13 sequence, but this is not significant over most of the expected range, and may not be worth the added processing required.

The minimum delay spread for these short sequences is much less than the desired 12.5 ms; recall that increasing the delay range by inserting longer null periods between the sequences results in larger Doppler spread ranges. This provides a good deal of flexibility in designing an HF sounding waveform, and in making small modifications for operation in different types of conditions, e.g., polar vs. mid-latitude.

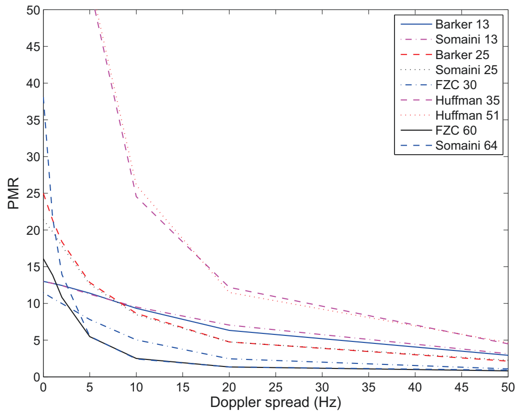


(a) Doppler shift 0 Hz

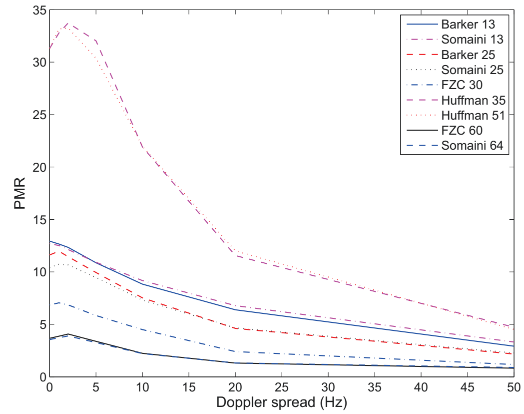


(b) Doppler shift 2 Hz

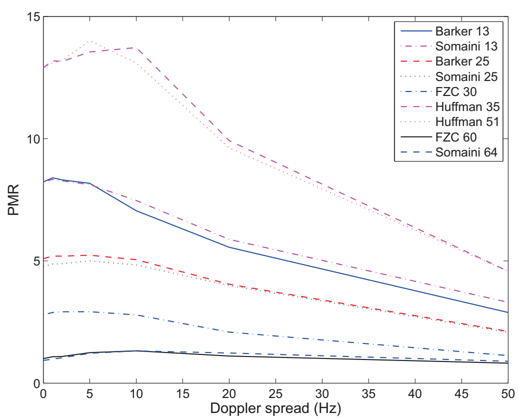


(c) Doppler shift 5 Hz

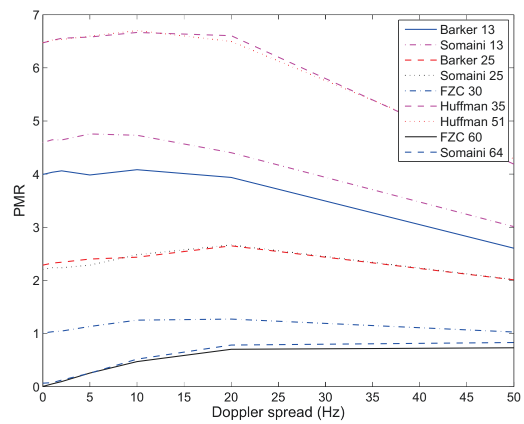


(d) Doppler shift 10 Hz

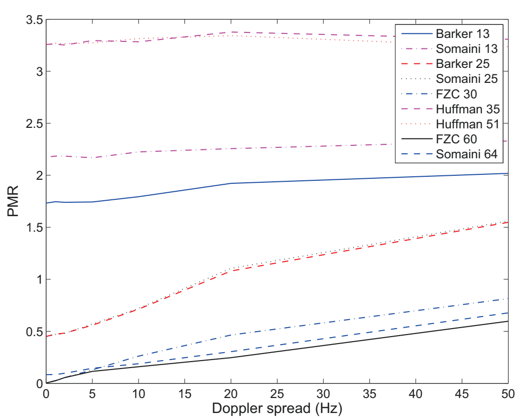


(e) Doppler shift 20 Hz

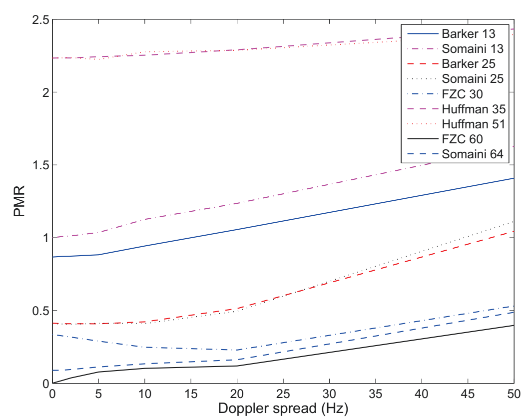


(f) Doppler shift 30 Hz

***Figure 4:*** *Peak-to-maximum sidelobe ratio of aperiodic sequences, 2400 baud.*

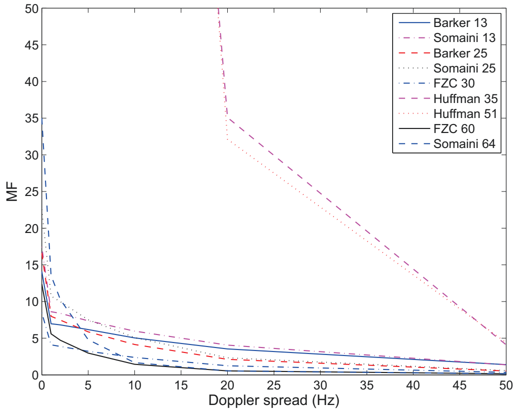


(a) Doppler shift 0 Hz

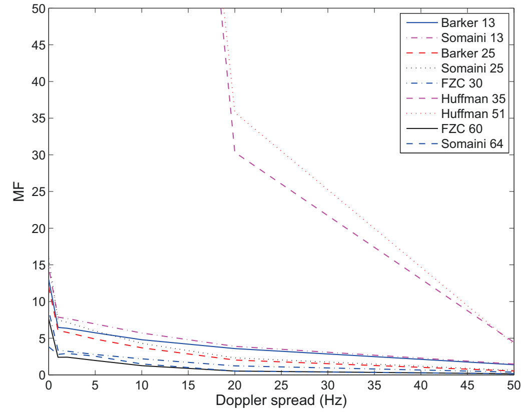


(b) Doppler shift 2 Hz

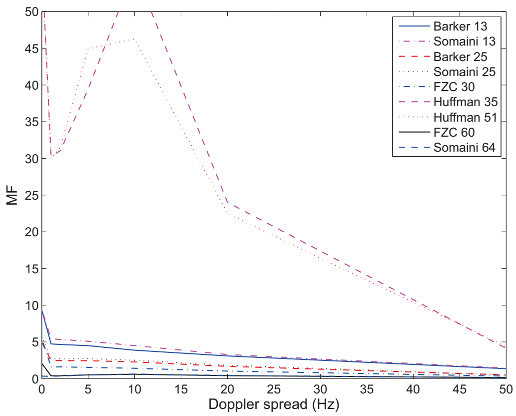


(c) Doppler shift 5 Hz

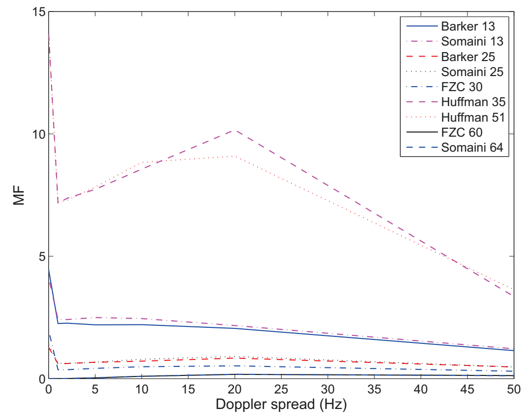


(d) Doppler shift 10 Hz

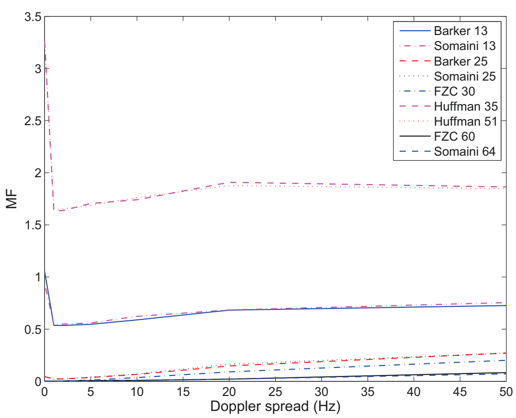


(e) Doppler shift 20 Hz

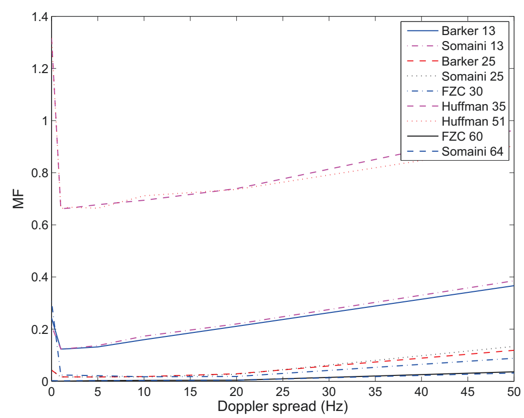


(f) Doppler shift 30 Hz

***Figure 5:*** *Merit factor of aperiodic sequences, 2400 baud.*

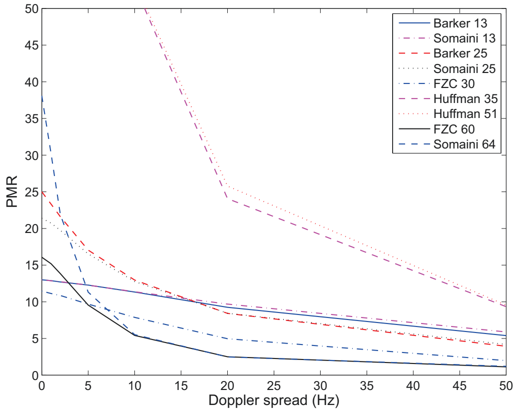


(a) Doppler shift 0 Hz

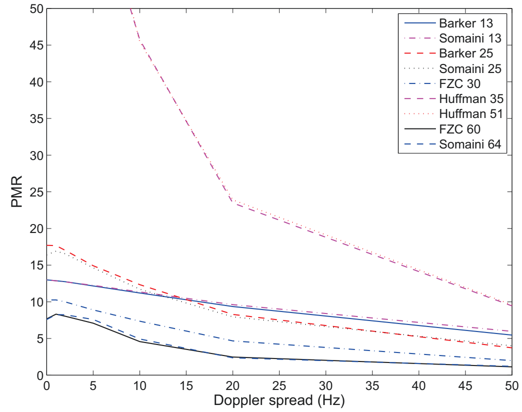


(b) Doppler shift 2 Hz

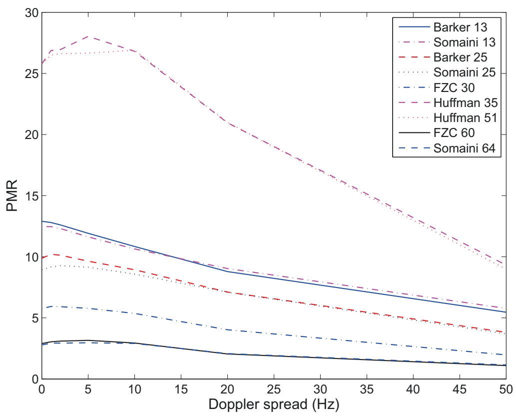


(c) Doppler shift 5 Hz

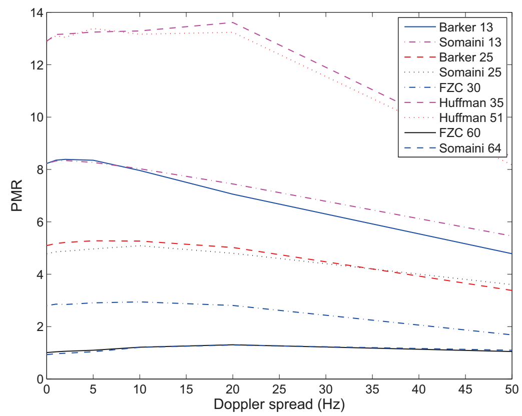


(d) Doppler shift 10 Hz

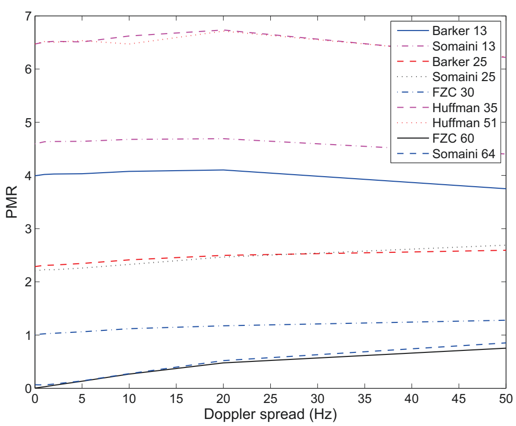


(e) Doppler shift 20 Hz

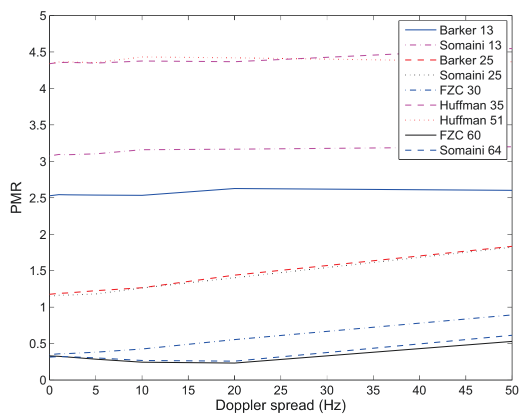


(f) Doppler shift 30 Hz

***Figure 6:*** *Peak-to-maximum sidelobe ratio of aperiodic sequences, 9600 baud.*

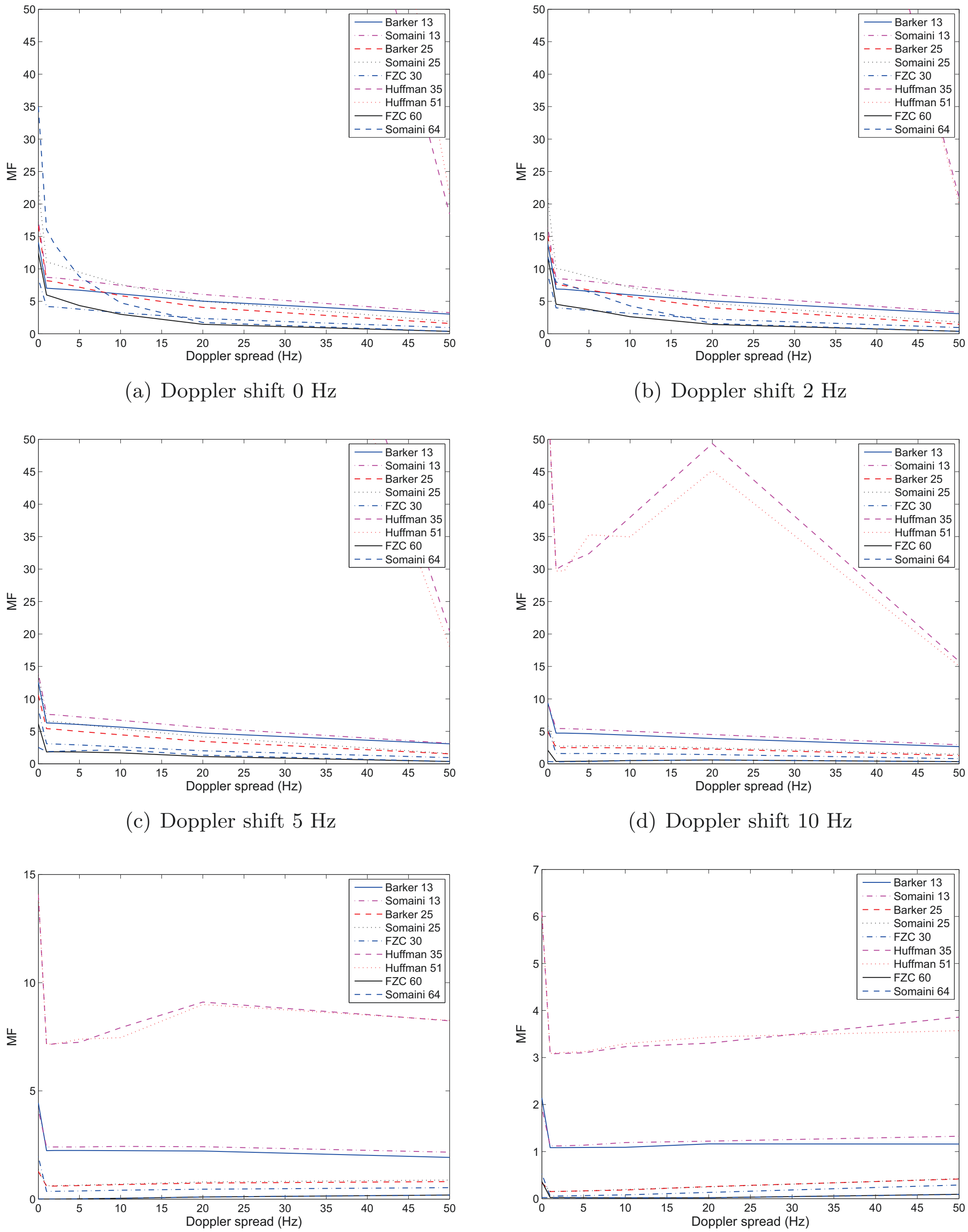


(a) Doppler shift 0 Hz

(b) Doppler shift 2 Hz

(c) Doppler shift 5 Hz

(d) Doppler shift 10 Hz

(e) Doppler shift 20 Hz

(f) Doppler shift 30 Hz

***Figure 7:*** *Merit factor of aperiodic sequences, 9600 baud.*

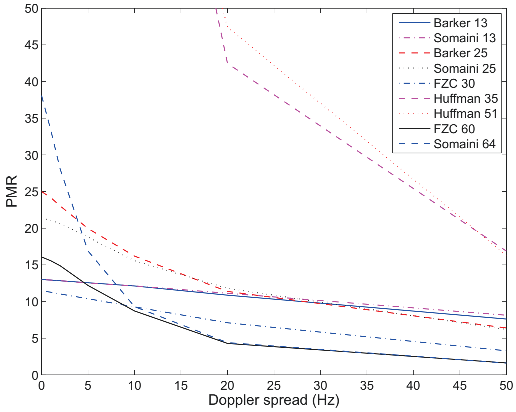


(a) Doppler shift 0 Hz

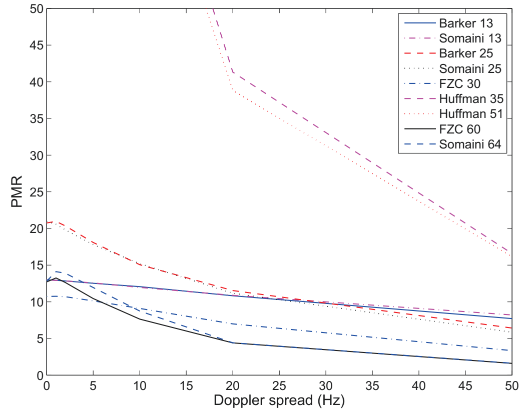


(b) Doppler shift 2 Hz

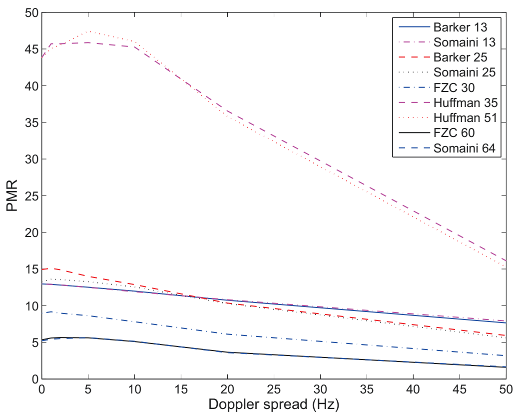


(c) Doppler shift 5 Hz

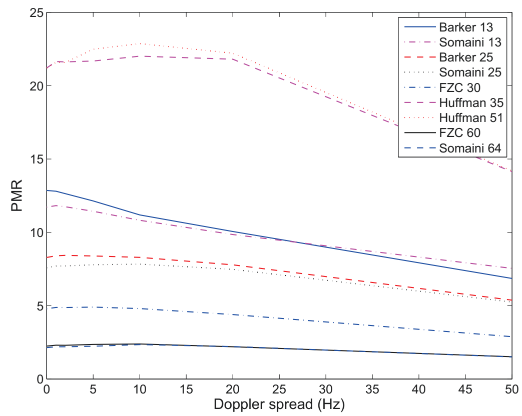


(d) Doppler shift 10 Hz

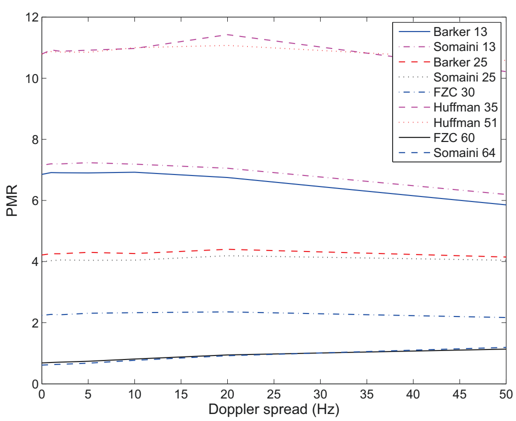


(e) Doppler shift 20 Hz

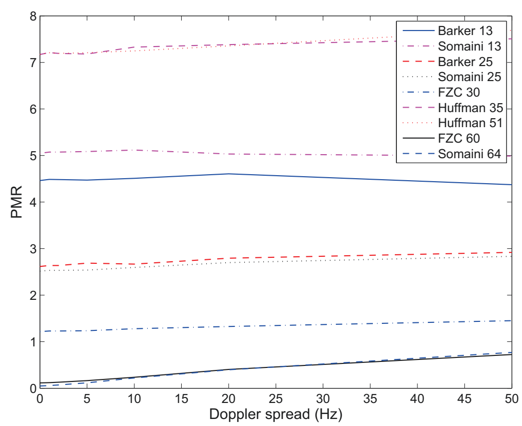


(f) Doppler shift 30 Hz

***Figure 8:*** *Peak-to-maximum sidelobe ratio of aperiodic sequences, 24000 baud.*

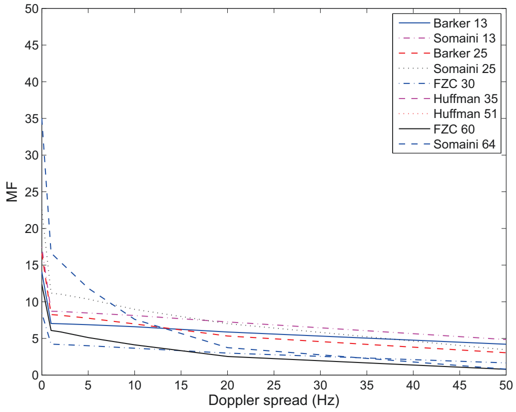


(a) Doppler shift 0 Hz

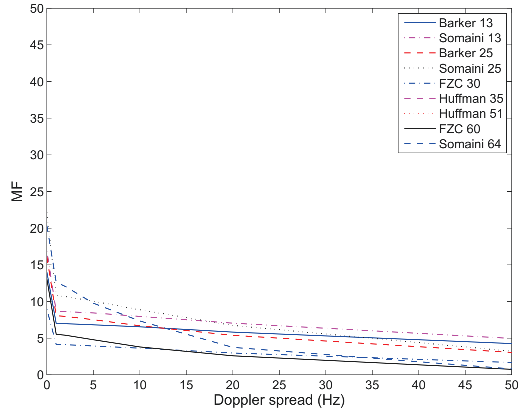


(b) Doppler shift 2 Hz

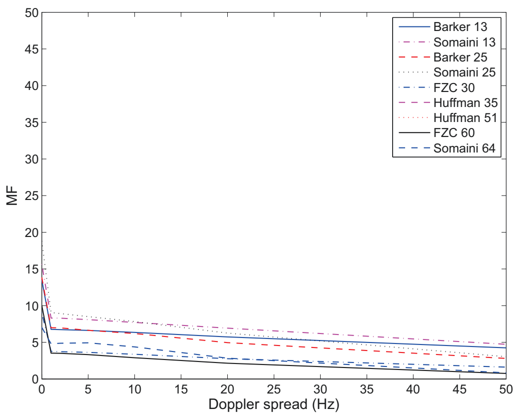


(c) Doppler shift 5 Hz

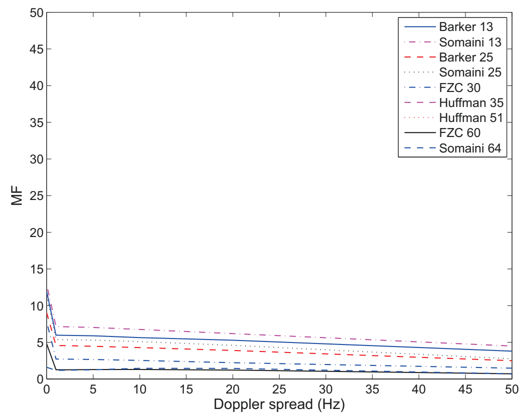


(d) Doppler shift 10 Hz

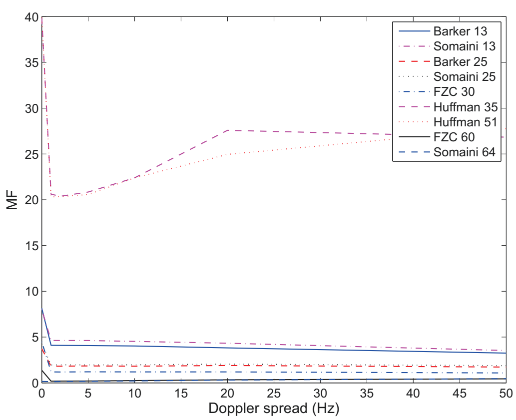


(e) Doppler shift 20 Hz

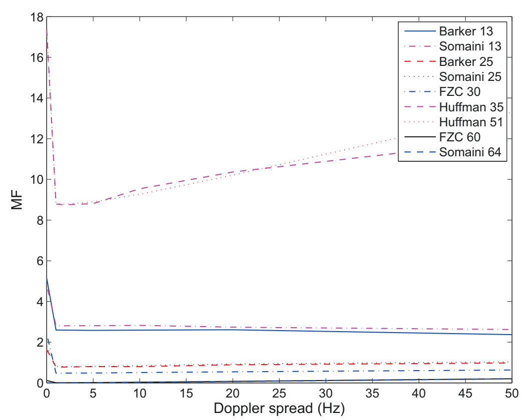


(f) Doppler shift 30 Hz

***Figure 9:*** *Merit factor of aperiodic sequences, 24000 baud.*

## 4.5 Periodic sequences

The characteristics of the ACFs of the periodic sequences considered are summarised in Table 3. The corresponding delay and Doppler spread ranges are shown in Table 4, and the PMR and MF measured using simulations of unimodal Gaussian fading distributions with different Doppler shifts $f_D$ and Doppler spreads $2\sigma$ are shown for $B = 2400$, $B = 9600$ and $B = 24k$ in Figures 10 to 13.

As with the aperiodic sequences, the shortest m-sequence provides the most consistent performance over a wide range of channel distortions, but it has a correspondingly small processing gain, related to the small PMR and MF values. In contrast, the longest m-sequence generally degrades rapidly with increasing Doppler spread, except at high Doppler shifts, where the changing phase due to frequency offset counters the impact of randomness due to fading, on average.

In spite of the widespread use of these sequences in characterising mobile UHF channels, the delay-Doppler characteristics illustrate their unsuitability for high-latitude HF, as none are able to meet both the delay and Doppler spread requirements. Unlike the aperiodic sequences, there is no flexibility to trade-off these features, as the periodic sequences must be transmitted consecutively to achieve their desirable ACF characteristics.

***Table 3:*** *General ACF characteristics of periodic sequences.*

| sequence | ideal PMR | ideal MF | PG (dB) |
|---|---|---|---|
| m-sequence 7 | 7 | 4.1 | 8.5 |
| m-sequence 15 | 15 | 8.0 | 11.8 |
| m-sequence 31 | 31 | 16.0 | 14.9 |
| m-sequence 63 | 63 | 32.0 | 18.0 |

***Table 4:*** *General delay-Doppler characteristics of periodic sequences.*

| sequence | minimum $T$ (ms) | | | maximum Doppler spread (Hz) | | |
|---|---|---|---|---|---|---|
| | $B = 2400$ | $B = 9600$ | $B = 24k$ | $B = 2400$ | $B = 9600$ | $B = 24k$ |
| m-sequence 7 | 2.9 | 0.7 | 0.3 | 171.4 | 685.7 | 1714.3 |
| m-sequence 15 | 6.3 | 1.6 | 0.6 | 80.0 | 320.0 | 800.0 |
| m-sequence 31 | 12.9 | 3.2 | 1.3 | 38.7 | 154.8 | 387.1 |
| m-sequence 63 | 26.3 | 6.6 | 2.6 | 19.0 | 76.2 | 190.5 |

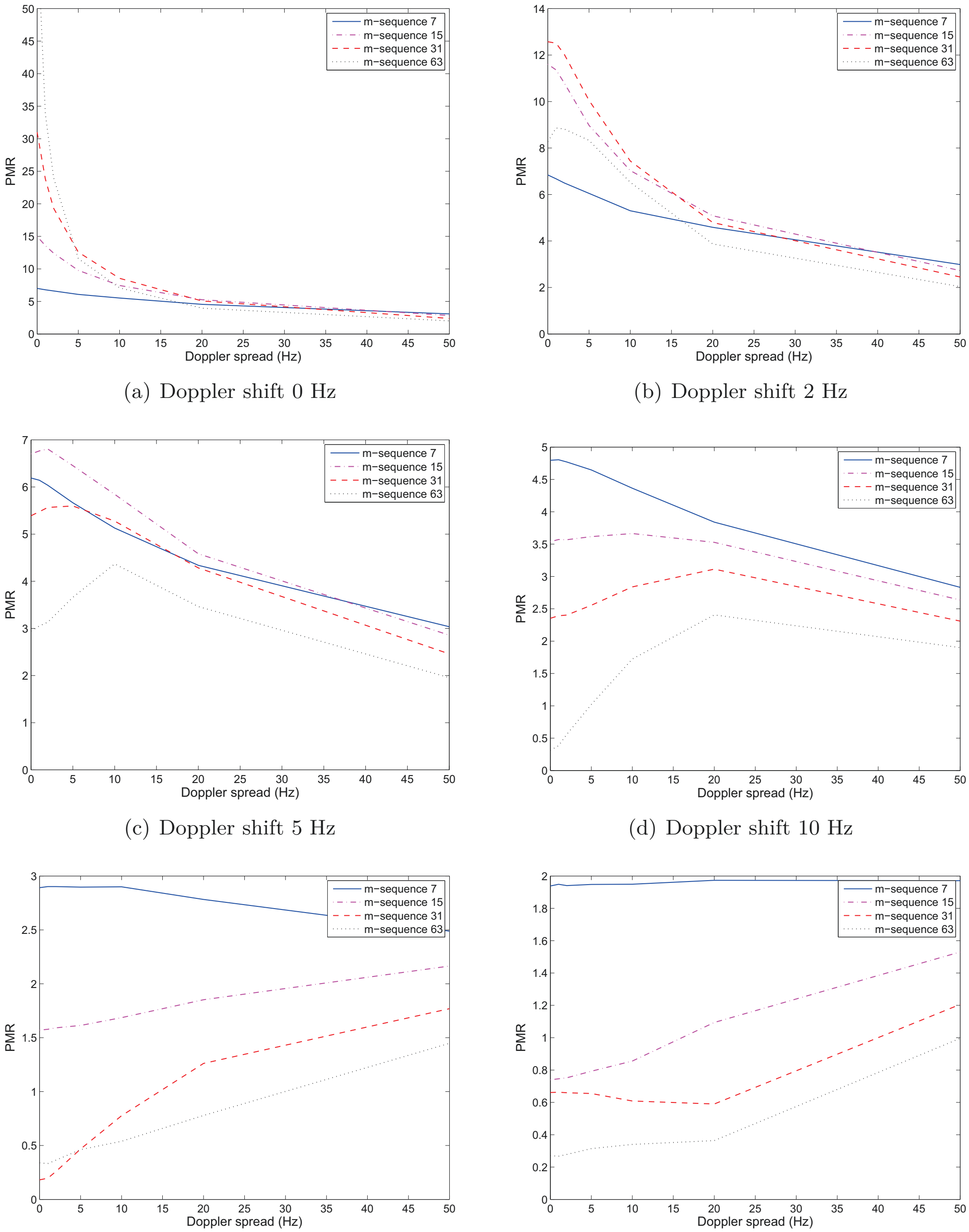


(a) Doppler shift 0 Hz

(b) Doppler shift 2 Hz

(c) Doppler shift 5 Hz

(d) Doppler shift 10 Hz

(e) Doppler shift 20 Hz

(f) Doppler shift 30 Hz

***Figure 10:*** *Peak-to-maximum sidelobe ratio of periodic sequences, 2400 baud.*

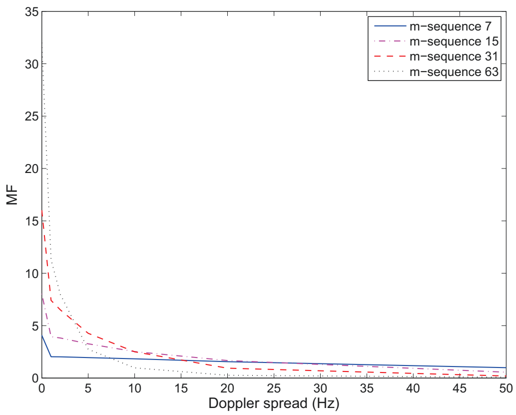


(a) Doppler shift 0 Hz

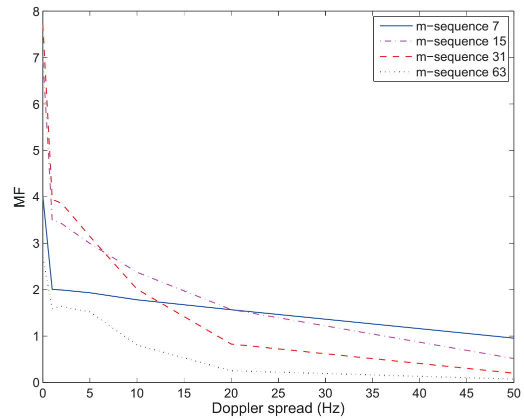


(b) Doppler shift 2 Hz

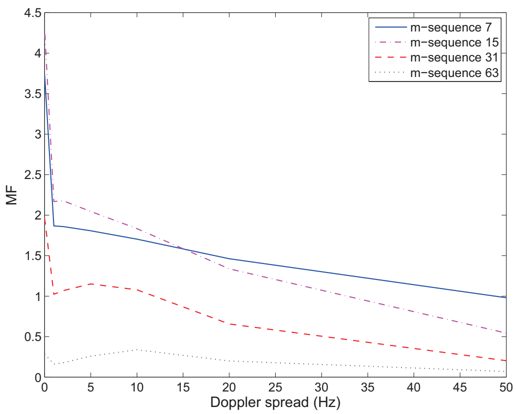


(c) Doppler shift 5 Hz

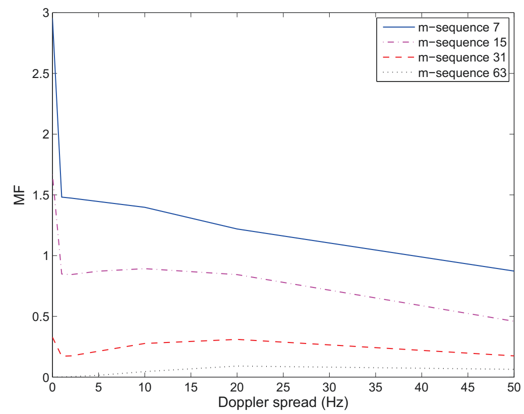


(d) Doppler shift 10 Hz

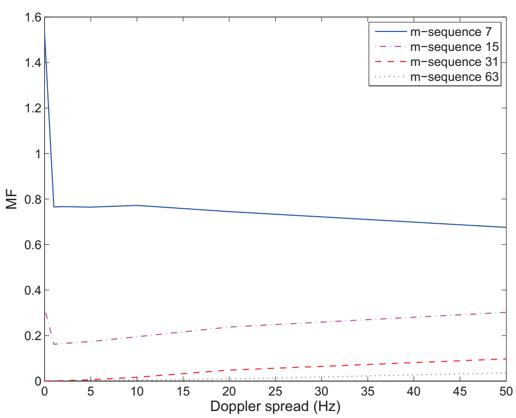


(e) Doppler shift 20 Hz

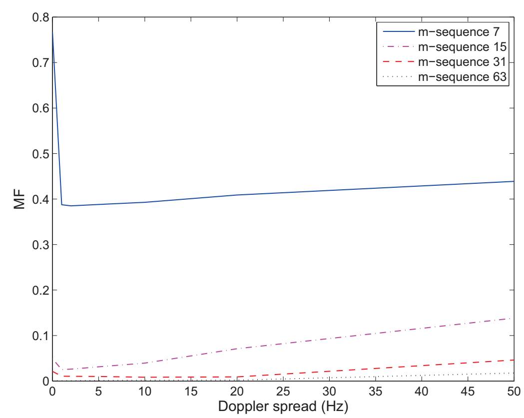


(f) Doppler shift 30 Hz

***Figure 11:*** *Merit factor of periodic sequences, 2400 baud.*

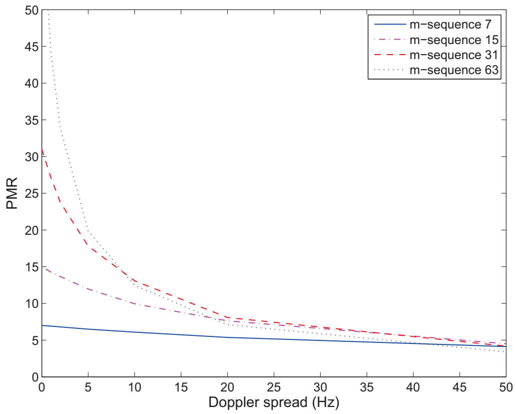


(a) Doppler shift 0 Hz

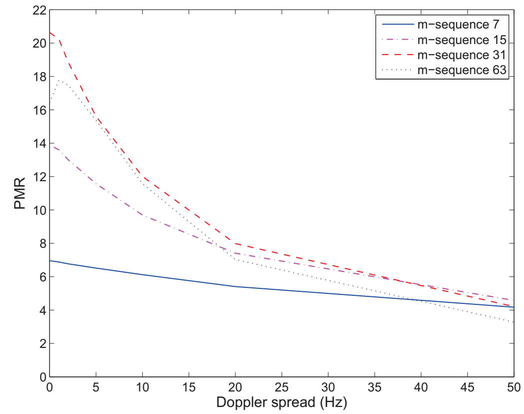


(b) Doppler shift 2 Hz

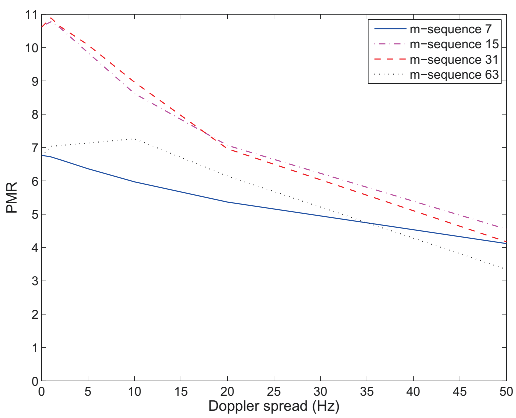


(c) Doppler shift 5 Hz

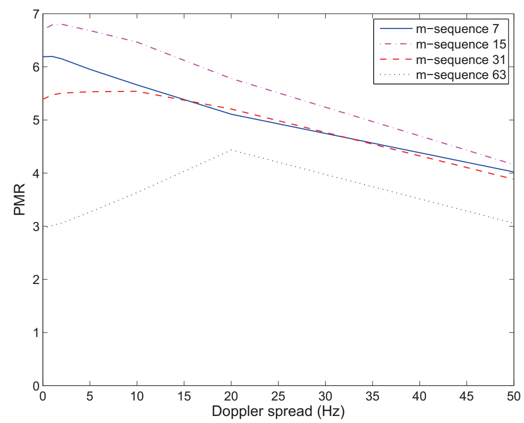


(d) Doppler shift 10 Hz

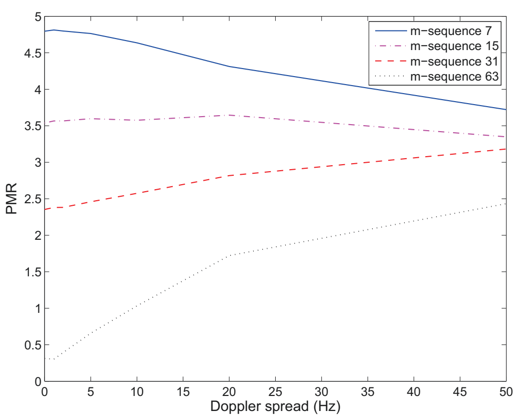


(e) Doppler shift 20 Hz

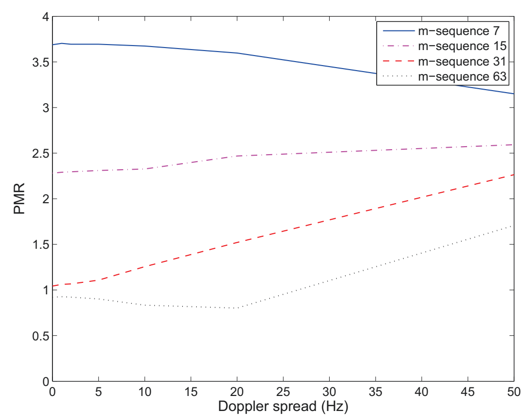


(f) Doppler shift 30 Hz

***Figure 12:*** *Peak-to-maximum sidelobe ratio of periodic sequences, 9600 baud.*

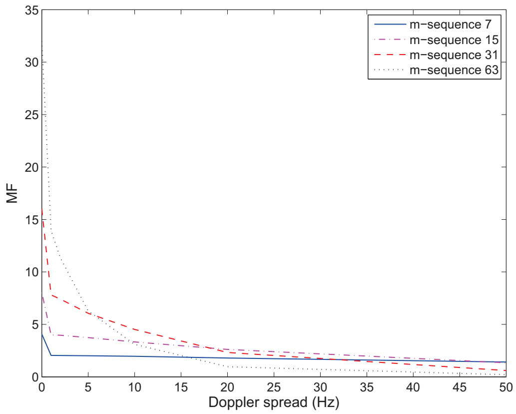


(a) Doppler shift 0 Hz

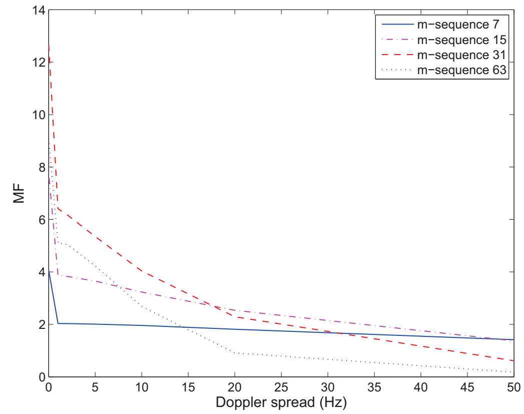


(b) Doppler shift 2 Hz

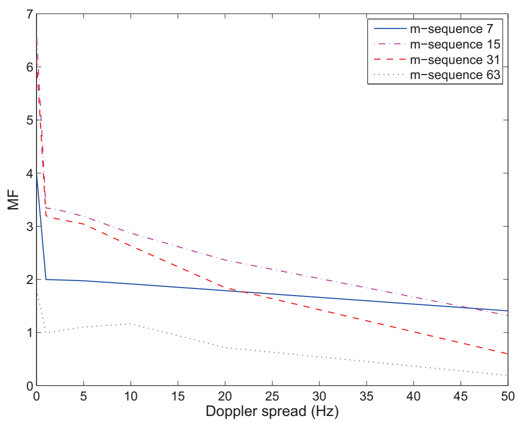


(c) Doppler shift 5 Hz

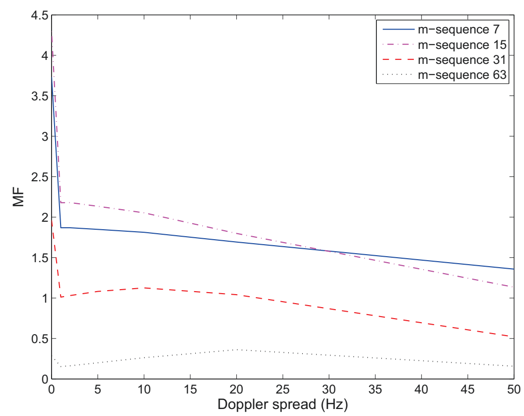


(d) Doppler shift 10 Hz

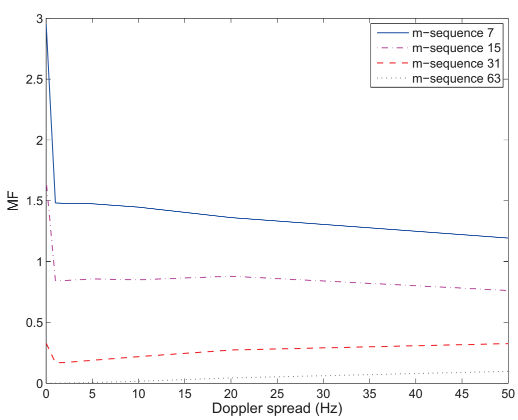


(e) Doppler shift 20 Hz

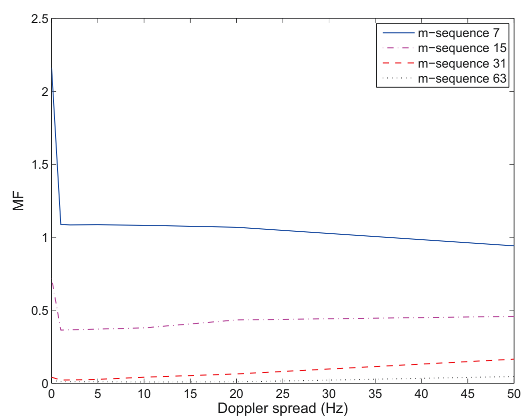


(f) Doppler shift 30 Hz

***Figure 13:*** *Merit factor of periodic sequences, 9600 baud.*

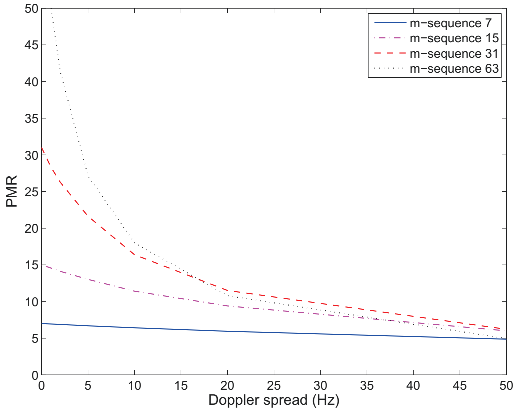


(a) Doppler shift 0 Hz

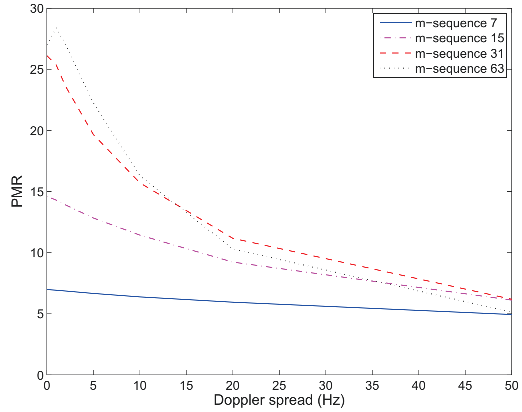


(b) Doppler shift 2 Hz

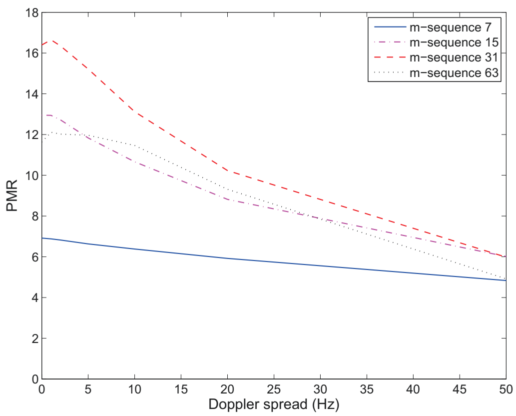


(c) Doppler shift 5 Hz

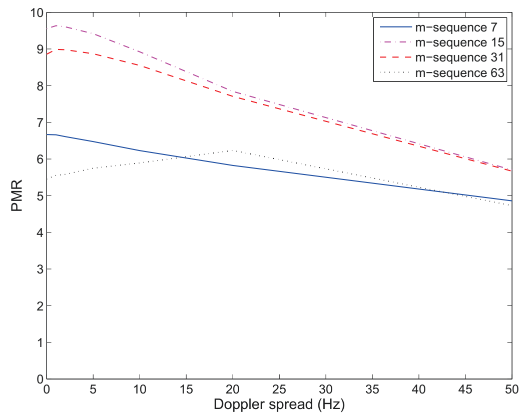


(d) Doppler shift 10 Hz

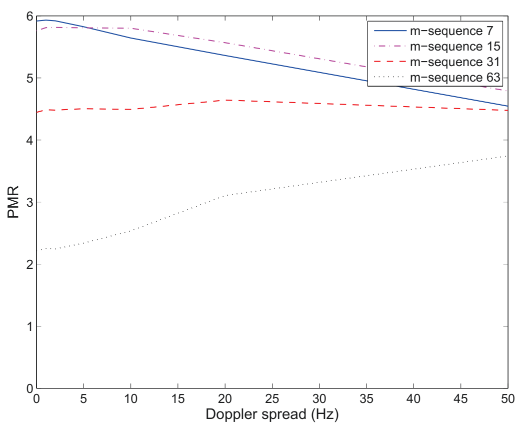


(e) Doppler shift 20 Hz

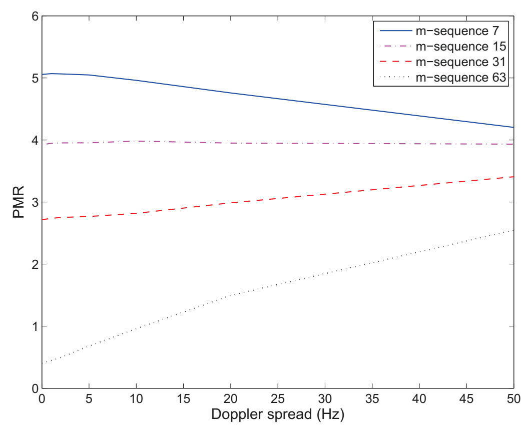


(f) Doppler shift 30 Hz

***Figure 14:*** *Peak-to-maximum sidelobe ratio of periodic sequences, 24000 baud.*

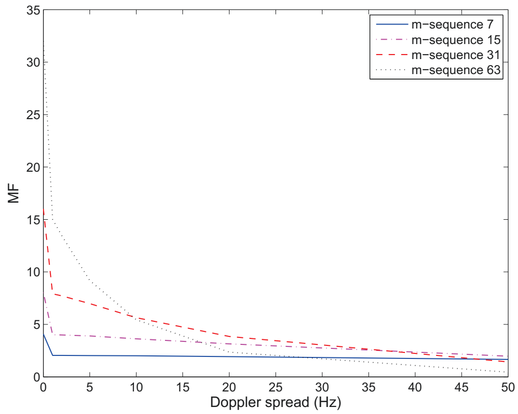


(a) Doppler shift 0 Hz

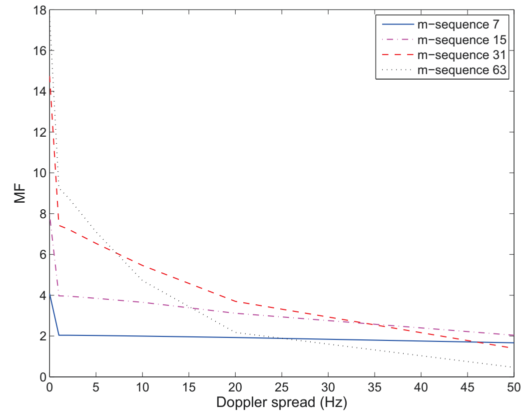


(b) Doppler shift 2 Hz

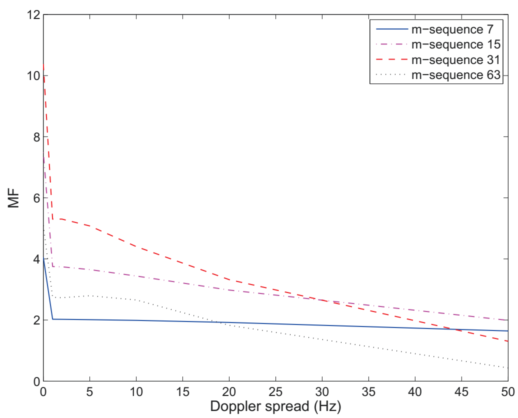


(c) Doppler shift 5 Hz

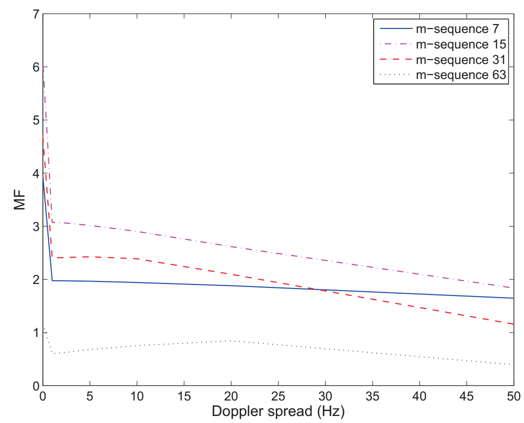


(d) Doppler shift 10 Hz

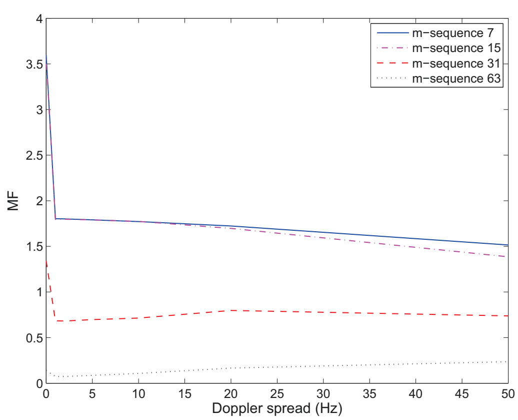


(e) Doppler shift 20 Hz

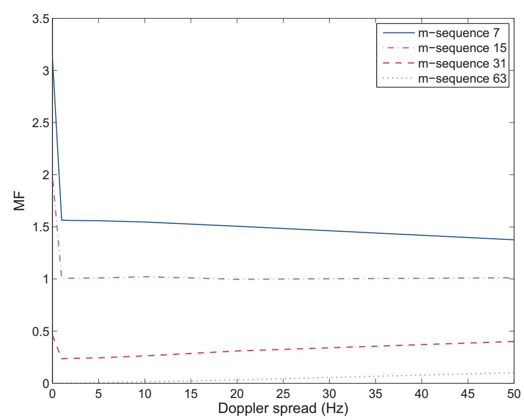


(f) Doppler shift 30 Hz

***Figure 15:*** *Merit factor of periodic sequences, 24000 baud.*

# 5 A note about coherence time

As summarised above, the delay and Doppler conditions observed on high latitude paths are highly variable. It was noted after (6) that the channel response estimation technique relies on the assumption that $h(n,\ell) = h(\ell)$, in other words, that channel response remains constant over the length of the pseudo-noise sequence correlation. In highly disturbed conditions, this may not be true, especially for long sequences. Understanding how much the real channel varies from the assumed model is important in the design of channel sounders, as it determines parameters such as integration time.

When the transmitted signal is affected by Doppler shift or fading, the channel response is time-dependent. Using the formulation in [52], the channel response at time $n+i$ can be written in terms of the response at time $n$ as follows

$$h(n+i,\ell) = \rho_{\ell,i} h(n,\ell) - e(n,i,\ell) \tag{16}$$

where $\rho_i$ is the correlation coefficient of the channel response for tap-delay $\ell$ over $i$ intervals, and $e(n,i,\ell)$ is an offset or error reflecting the variation of the channel response from the average correlation profile. The random variables $e$ are independent and identically distributed with mean zero, and variance $\sigma^2_{e_{\ell,i}} = (1-|\rho_{\ell,i}|^2)\sigma^2_{h_\ell}$. Also, $e(n,i,\ell)$ and $h(n,\ell)$ are uncorrelated.

The HF channel is generally modelled as a tapped-delay line where each tap is Rayleigh fading with a Gaussian power spectrum [34], i.e.,

$$S_H(\omega,\ell) = |H(\omega,\ell)|^2 = \frac{1}{\sqrt{2\pi}\sigma_{h,\ell}} \exp\left[\frac{-(f-f_{D,\ell})^2}{2\sigma^2_{h,\ell}}\right] \tag{17}$$

where $H(\omega,\ell)$ is the Fourier transform of $h(n,\ell)$, and $f_{D,\ell}$ and $2\sigma_{h,\ell}$ are the Doppler shift and spread of tap $\ell$, respectively. The Doppler spread is computed from $\sigma^2_{h_\ell} = \mathcal{E}\{|h(m,\ell)|^2\}$.

As shown by Rice [53], with the wide-sense stationarity assumption, the correlation function can be derived from the inverse Fourier transform of the power spectrum, which in this case is also a Gaussian function, i.e.,

$$R_\ell(\tau) = \mathcal{F}^{-1}\{S_H(\omega,\ell)\} = \frac{1}{\sqrt{2\pi}} \exp\left[-\frac{\sigma^2_{h,\ell}\tau^2}{2} + jf_{D,\ell}\tau\right]. \tag{18}$$

The correlation coefficient $\rho_{\ell,i}$ can then be computed for the appropriate delay $\tau = i\Delta t$ as

$$\rho_{\ell,i} = \frac{R_\ell(\tau)}{R_\ell(0)} = \exp\left[-\frac{\sigma^2_{h,\ell}\tau^2}{2}\right] \cdot \exp\left[jf_{D,\ell}\tau\right] \tag{19}$$

where the first term determines the absolute value of $\rho_{\ell,i}$, and the second defines its phase. Thus, in the absence of Doppler shift, the correlation coefficient is real-valued.

Then the receiver correlation in (6b) is

$$
\begin{aligned}
\phi_{rs}(-m) \quad = \quad & \sum_{\ell=0}^{L_{max}} \sum_{i=1}^{K} h(m,\ell) s(m+i-\ell) s^*(i) - && (20)\\
& \quad \sum_{\ell=0}^{L_{max}} \sum_{i=1}^{K} (1-\rho_{\ell,i}) h(m,\ell) s(m+i-\ell) s^*(i) + && (21)\\
& \quad \sum_{\ell=0}^{L_{max}} \sum_{i=1}^{K} e(m+i,i,\ell) s(m+i-\ell) s^*(i) + \ nu(m).
\end{aligned}
$$

For a sequence with an ideal impulse ACF, this becomes

$$\phi_{rs}(-m) = \sum_{\ell=0}^{L_{max}} h(m,\ell)\phi_{ss}(m-\ell) - \sum_{\ell=0}^{L_{max}} P_\ell + \sum_{\ell=0}^{L_{max}} D_\ell + \nu(m) \tag{22}$$

where the first term is the desired channel response estimate, and

$$P_\ell = h(m,\ell) \sum_{i=1}^{K} (1-\rho_{\ell,i}) s(m+i-\ell) s^*(i) \tag{23}$$

and

$$D_\ell = \sum_{i=1}^{K} e(m+i,i,\ell) s(m+i-\ell) s^*(i) \tag{24}$$

are uncorrelated distortion components, and $\nu(m)$ is the noise.

As $h$ represents a fading channel, $\mathcal{E}\{h(m,\ell)\} = 0$, hence $\mathcal{E}\{P_\ell\} = 0$. Writing the distorted correlation function as

$$\psi_{ss}(m,\ell) = \sum_{k=1}^{K} (1-\rho_{\ell,k}) s(k) s^*(k-m) \tag{25}$$

the variance of this component is

$$\mathcal{E}\{|P_\ell|^2\} = \sigma_{h,\ell}^2 \left|\psi_{ss}(m,\ell)\right|^2. \tag{26}$$

Also $\mathcal{E}\{D_\ell\} = 0$ as the error $e$ has zero mean, and

$$\mathcal{E}\{|D_\ell|^2\} = \sum_{i=1}^{K} \sigma_{\ell,i}^e |s(m+i-\ell)|^2 |s(i)|^2 \tag{27}$$

which, for unit envelope sequences ($|s(k)|^2 = 1$ for $k = 1, \ldots, K$) becomes

$$\mathcal{E}\{|D_\ell|^2\} = \sigma_{h,\ell}^2 \sum_{i=1}^{K} (1-|\rho_{\ell,i}|^2). \tag{28}$$

These two distortion components illustrate how the structure of the sequence, as well as its length, impact its resilience in Doppler spread and shift.

The approximate values of the term $|1-\rho_i|$, which appears in the distortion equation (26), are shown in Table 5 for a range of Doppler spreads and delays, assuming a unimodal Gaussian fading distribution (17), as in [34]. As seen in Tables 1 and 3, the sequence intervals $T$ range from 10.4 to 52.9 ms for the aperiodic sequences, and up to 16.3 ms for the periodic ones at 2400 baud.

Table 6 shows the values $\sum_i(1-|\rho_i|^2)$, which appears in (28), for different baud rates and sequence lengths. When there is also Doppler shift, as given by (19), the absolute values in both tables remain the same, but $\rho$ takes complex values.

***Table 5:*** *Approximate correlation coefficient terms* $|1-\rho|$ *in* (26).

| Doppler spread (Hz) | delay (ms) 0.4 | 1.6 | 3.2 | 6.4 | 9.6 | 12.8 |
|---|---|---|---|---|---|---|
| 1 | $2.00\,10^{-8}$ | $3.20\,10^{-7}$ | $1.28\,10^{-6}$ | $5.12\,10^{-6}$ | $1.15\,10^{-5}$ | $2.05\,10^{-5}$ |
| 2 | $8.0\,10^{-8}$ | $1.28\,10^{-6}$ | $5.12\,10^{-6}$ | $2.05;10^{-5}$ | $4.61\,10^{-5}$ | $8.19\,10^{-5}$ |
| 5 | $5.00\,10^{-7}$ | $8.00\,10^{-6}$ | $3.20\,10^{-5}$ | $1.28\,10^{-4}$ | $2.88\,10^{-4}$ | $5.12\,10^{-4}$ |
| 10 | $2.00\,10^{-6}$ | $3.20\,10^{-5}$ | $1.28\,10^{-4}$ | $5.12\,10^{-4}$ | $1.15\,10^{-3}$ | $2.05\,10^{-3}$ |
| 20 | $8.00\,10^{-6}$ | $1.28\,10^{-4}$ | $5.12\,10^{-4}$ | $2.05\,10^{-3}$ | $4.60\,10^{-3}$ | $8.16\,10^{-3}$ |
| 50 | $5.00\,10^{-5}$ | $8.00\,10^{-4}$ | $3.19\,10^{-3}$ | $1.27\,10^{-2}$ | $2.84\,10^{-2}$ | $5.00\,10^{-2}$ |

***Table 6:*** *Approximate correlation coefficient terms* $\sum_{i=1}^{\tilde{K}}|\rho_i|^2$ *in* (28).

| Doppler spread (Hz) | $\tilde{K}=15$ baud rate $2.4k$ | $9.6k$ | $24k$ | $\tilde{K}=25$ baud rate $2.4k$ | $9.6k$ | $24k$ | $\tilde{K}=35$ baud rate $2.4k$ | $9.6k$ | $24k$ |
|---|---|---|---|---|---|---|---|---|---|
| 1 | $5.4\,10^{-5}$ | $3.4\,10^{-6}$ | $5.4\,10^{-7}$ | $2.4\,10^{-4}$ | $1.5\,10^{-5}$ | $2.4\,10^{-6}$ | $6.5\,10^{-4}$ | $4.0\,10^{-5}$ | $6.5\,10^{-6}$ |
| 2 | $2.2\,10^{-4}$ | $1.3\,10^{-5}$ | $2.2\,10^{-6}$ | $9.6\,10^{-4}$ | $6.0\,10^{-5}$ | $9.6\,10^{-6}$ | $2.6\,10^{-3}$ | $1.6\,10^{-4}$ | $2.6\,10^{-5}$ |
| 5 | $1.3\,10^{-3}$ | $8.4\,10^{-5}$ | $1.3\,10^{-5}$ | $6.0\,10^{-3}$ | $3.7\,10^{-4}$ | $6.0\,10^{-5}$ | $1.6\,10^{-2}$ | $1.0\,10^{-3}$ | $1.6\,10^{-4}$ |
| 10 | $5.4\,10^{-3}$ | $3.4\,10^{-4}$ | $5.4\,10^{-5}$ | $2.4\,10^{-2}$ | $1.5\,10^{-3}$ | $2.4\,10^{-4}$ | $6.5\,10^{-2}$ | $4.0\,10^{-3}$ | $6.5\,10^{-4}$ |
| 20 | $2.2\,10^{-2}$ | $1.3\,10^{-3}$ | $2.2\,10^{-4}$ | $9.6\,10^{-2}$ | $6.0\,10^{-3}$ | $9.6\,10^{-4}$ | $2.6\,10^{-1}$ | $1.6\,10^{-2}$ | $2.6\,10^{-3}$ |
| 50 | $1.3\,10^{-1}$ | $8.4\,10^{-3}$ | $1.3\,10^{-3}$ | $5.9\,10^{-1}$ | $3.7\,10^{-2}$ | $6.0\,10^{-3}$ | 1.6 | $1.0\,10^{-1}$ | $1.6\,10^{-2}$ |

Tables 5 and 6 show the large impact that Doppler spread has, by decorrelating the channel response over short intervals. By way of comparison, the channel coherence time, defined as the time over which the channel can be considered unchanging, is often measured based on the analysis by Gans [54], which measured the coherence bandwidth/interval as the frequency/time at which the correlation dropped to 0.75. Cox used values of 0.9 and 0.5 to evaluate the coherence bandwidth of measured data [55]. In [56], the threshold 0.5 is used. The lack of formal acceptance of a value, and of a clear understanding of the implications of the choice on any given system, mean that the concept of 'coherence time' is used imprecisely and loosely.

Table 7 shows the coherence time estimates for these different correlation values, assuming a unimodal Gaussian fading distribution.

***Table 7:*** *Coherence time estimates $T_c$ for different correlation thresholds.*

| Doppler spread (Hz) | Coherence time estimate (ms) for $\rho = 0.9$ | $\rho = 0.7.5$ | $\rho = 0.5$ |
|---|---|---|---|
| 1 | 918 | 1520 | 2350 |
| 2 | 460 | 760 | 1180 |
| 5 | 180 | 300 | 470 |
| 10 | 92 | 152 | 235 |
| 20 | 46 | 76 | 118 |
| 50 | 18 | 30 | 47 |

Based on the performance of the pseudo-noise sequences over the range of Doppler spreads up to 50 Hz, it is apparent that using the common rule-of-thumb values for coherence time are inadequate for specifying the selection of the sounding waveform. For example, the longest m-sequence considered, with a repetition interval of 16.3 ms at 2400 baud which has a correlation value of $\rho = 0.92$, would easily be considered within the coherence time for Doppler spreads up to and exceeding 50 Hz according to Table 7, but as seen in Tables 5 and 6 and the results from simulations (Figure 10), the PMR decreases precipitously as the Doppler spread increases and the MF is less than one for Doppler spread 50 Hz with no Doppler shift.

Thus, in defining a sounding system, a the temporal correlation must be considered carefully, as the impacts of distortion due to time-varying amplitude and phase are considerable, as observed in the simulation results presented in Section 4. It is important not to rely on the common rule-of-thumb for coherence times in determining practical sequence lengths.

# 6 Recommendations

The range of delay and Doppler conditions observed on high latitude BLOS HF channels means that sounding waveforms must be carefully selected.

The core of the sounding waveform should be a pseudo-noise sequence, transmitted repeatedly at fixed intervals, which will be processed to generate a delay-Doppler spectrogram. This supports the extraction of the key parameters required: received SNR, number and relative delays of propagating modes; and, for each mode, relative power, delay spread, Doppler shift and Doppler spread.

Precise time-of-flight measurements are not generally required for evaluating HF radios, but a TOF mode similar to the delay-Doppler mode with a longer repetition interval would help to resolve aliasing in the time domain, in cases where the delay range exceeds that provided by the delay-Doppler repetition interval in the delay-Doppler mode. Similarly, a continuous wave mode allows deconfliction of aliased Doppler characteristics if the delay-

Doppler repetition interval is too long, resulting in an insufficient Doppler range.

The aperiodic sequences are the best choice for pseudo-noise sequences, because the null interval can be selected to trade-off the delay and Doppler ranges as desired, to a degree. The longer sequences suffer most distortion, limiting their useful range. The Barker 13 sequence was used in the DAMSON 3 kHz system, and the analysis here shows that was a good choice. The Barker 25 sequence was selected for the 12 kHz (9600 baud) sounder system implementation: for the most extreme conditions, the shorter sequences may have been a more suitable choice. Even for wideband HF, the shortest sequences were the most robust, even though they have a very small processing gain. There is a small gain in using the complex Somaini 13 in place of the Barker 13.

Transmitting a large number of pseudo-noise sequences, over many seconds or even minutes, would enable more detailed analyses of the fading model and the dynamic nature of the channel than have been achieved to-date. Care must be taken to analyse the resulting data for wide-sense stationarity – the results of this analysis would also be a useful contribution to knowledge base about high-latitude HF channels. Both would vastly improve the quality of HF channel simulators available, and would facilitate more accurate laboratory evaluation of radio technology.

# 7 Conclusions

The propagation parameters of the high-latitude BLOS HF channel have been measured in previous extensive campaigns. Not only can the conditions in auroral and polar regions be extreme, they also vary quite rapidly, especially during geomagnetically active periods. To measure and compare radio performance over these links is challenging, as there is no guarantee that any two radios are experiencing the same propagation conditions, even when averaged over a period of days or weeks. While testing radios on nearby frequency channels would expose them to similar propagating conditions, they may not have to deal with the extreme multipath spreads, Doppler spreads and shifts that are experienced during geomagnetic storms.

To evaluate and compare radio technologies fairly, then, it is preferable that simulated or emulated channels be used for some part of the evaluation, so that conditions can be controlled and repeated, and the full range of operational conditions can be tested. To properly parameterise these models, measured data is required to ensure an appropriate range of conditions is considered.

The DAMSON project, a collaborative effort amongst Canada, UK, Norway and Sweden in the 1990's, collected propagation measurements from high-latitude paths in northern Europe, which were used to support analyses of the propagation physics, determine specifications for HF communications standards, and evaluate radio performance. The experience from that work provides a basis for the range of propagation conditions that might be experienced on other high-latitude BLOS links.

Pseudo-noise sequences are used in most mobile channel sounders, and in many prior HF sounding systems, as they can provide an impulse-like response with a uniform transmission power, using low-complexity signal processing. These responses can be combined to generate a characteristic function in time and frequency, from which the delay and Doppler parameters of each mode can be extracted. This work has evaluated periodic and aperiodic sequences for their suitability to measure HF modal characteristics in the extreme conditions experienced in polar and auroral regions.

Aperiodic sequences have been shown to be more suitable for HF sounding for high-latitude conditions, because their repetition interval can be adjusted to tune the trade-off between delay and Doppler ranges. Short, unit envelope sequences are more robust to the distortions resulting from Doppler shift and spread. Even though the longer sequences have higher processing gains and are thus able to be received in lower SNR channels, the distortion they experience counters this advantage. The shorter sequences are therefore preferred, even for wideband HF.

Combining the core pseudo-noise sequence transmissions with the ability for increased range in delay and frequency provides additional robustness to confirm observations in particularly severe conditions.

The Gaussian fading model has been assumed for HF channels for many years, but has not been validated for high-latitude measurements. For the sophisticated signal processing used in modern radios, understanding the expected fading model may be advantageous. More detailed measurements, providing higher statistical reliability and possibly higher resolution, would be useful to validate or modify the fading model in different operating conditions, and also could be used to develop time-varying models for enhanced channel simulation.

# References

[1] Innovative Solutions Canada, "Robust "beyond line of sight" (BLOS) communications in satellite-denied environments," https://www.ic.gc.ca/eic/site/101.nsf/eng/00015.html Accessed July 26, 2018.

[2] K. Davies, *Ionospheric Radio.* London, UK: Peter Peregrinus Ltd, 1990.

[3] H. G. Booker, P. K. Pasricha, and W. J. Powers, "Use of scintillation theory to explain frequency-spread on F-region ionograms," *J. Atmospheric and Terrestrial Physics*, vol. 48, no. 4, pp. 327–354, Apr. 1986.

[4] W. I. Axford and C. O. Hines, "A unifying theory of high-latitude geophysical phenomena and geomagnetic storms," *Canadian J. Physics*, vol. 39, no. 10, pp. 1433–1464, 1961.

[5] K. C. Yeh and G. W. Swenson, "F-region irregularities studied by scintillation of signals from satellites," *Radio Sci.*, vol. 68D, no. 8, Aug. 1964.

[6] R. D. Hunsucker and H. F. Bates, "Survey of polar and auroral region effects on HF propagation," *Radio Sci.*, vol. 4, no. 4, pp. 347–365, 1969.

[7] K. W. Moreland, T. J. Willink, G. O. Venier, P. S. Cannon, N. C. Davies, M. J. Angling, V. Jodalen, and B. Lundborg, "Comparison of mid-latitude and high-latitude HF channel measurements of doppler and multipath effects," in *Proc. Wireless*, vol. 2, 1995.

[8] E. M. Warrington and A. J. Stocker, "Measurements of the doppler and multipath spread of HF signals received over a path oriented along the midlatitude trough," *Rad. Sci.*, vol. 38, no. 5, 2003.

[9] A. J. Stocker, E. M. Warrington, and N. Y. Zaalov, "The effect of the mid-latitude trough on the direction of arrival and time-of-flight of HF radio signals," *Acta Geodaetica et Geophysica Hungarica*, vol. 37, no. 2-3, pp. 351–363, 2002.

[10] P. S. Cannon, M. J. Angling, N. C. Davies, T. Willink, V. Jodalen, B. Jacobson, B. Lundborg, and M. Broms, "Damson HF channel characterisation – a review," in *Proc. IEEE Mil. Commun. Conf. (MILCOM)*, vol. 1, Oct. 2000, pp. 59–64.

[11] T. J. Willink, N. C. Davies, J. Clarke, and M. B. Jorgenson, "Validation of HF channel simulators," in *Proc. IEE Colloq. on Freq. Sel. and Mgmt. Techn. for HF Commun.*, Feb. 1996.

[12] J. Goodman, J. Ballard, and E.Sharpe, "A long-term investigation of the HF communication channel over middle- and high-latitude paths," *Radio Sci.*, vol. 32, no. 4, pp. 1705–1715, 1997.

[13] “Canadian High Arctic Ionospheric Network,” chain.physics.unb.ca/chain/pages/cadi Accessed July 6, 2018.

[14] “Digisonde Station List,” www.digisonde.com/stationlist.html Accessed July 6, 2018.

[15] D. C. Coll and J. R. Storey, “Ionospheric sounding using coded pulse signals,” *Radio Sci. D*, vol. 68, pp. 1155–1159, 1964.

[16] L. S. Wagner, J. A. Goldstein, and E. A. Chapman, “Wideband HF channel prober: system description,” Naval Research Lab, Tech. Rep., Mar. 1983.

[17] L. S. Wagner, J. A. Goldstein, and W. D. Meyers, “Wideband probing of the transauroral HF channel: Solar minimum,” *Radio Sci.*, vol. 23, no. 4, pp. 555–568, Jul. 1988.

[18] N. C. Davies, P. S. Cannon, and M. J. Maundrell, “DAMSON – a system to measure multipath dispersion, Doppler spread and Doppler shift on HF communications channels,” in *Proc. IEE Colloq. High Latitude Ionospheric Propagation*, Apr. 1992.

[19] B. Lundborg, M. Bröms, P. S. Cannon, M. J. Angling, N. C. Davies, T. Willink, and V. Jodalen, “Measurements of doppler and multipath effects on high latitude HF paths,” in *Proc. Conf. on Radio Science and Telecommunications (RVK)*, vol. 96, 1996, pp. 345–349.

[20] M. Broms, B. Lundborg, V. Jodalen, and T. Bergsvik, “Doppler effects on high latitude HF paths during an ionospheric disturbance,” in *Proc. IEE Conf. HF Radio Systems and Techniques*, Jul. 1997, pp. 75–79.

[21] T. J. Willink and E. C. Landry, “Analysis of time-varying HF propagation characteristics,” in *Proc. IEE Conf. HF Radio Systems and Techniques*, Jul. 1997, pp. 70–74.

[22] D. C. Cox, “Delay Doppler characteristics of multipath propagation at 910 MHz in a suburban mobile radio environment,” *IEEE Trans. on Ant. and Prop.*, vol. 20, no. 5, pp. 625–635, Sep. 1972.

[23] R. J. C. Bultitude, S. A. Mahmoud, and W. A. Sullivan, “A comparison of indoor radio propagation characteristics at 910 MHz and 1.75 GHz,” *IEEE J. on Sel. Areas in Commun.*, vol. 7, no. 1, pp. 20–30, 1989.

[24] K. Kalliola, H. Laitinen, P. Vainikainen, M. Toeltsch, J. Laurila, and E. Bonek, “3-D double-directional radio channel characterization for urban macrocellular application,” *IEEE Trans. Ant. and Propag.*, vol. 51, no. 11, pp. 3122–3133, 2003.

[25] T. J. Willink, “MIMO OFDM for broadband fixed wireless access,” *IEE Proc.-Commun.*, vol. 152, no. 1, pp. 75–81, 2005.

[26] T. J. Willink and G. W. K. Colman, “Measurement-based analysis of cross-layer

adaptation for MIMO in mobile urban environments," *IET Communications*, vol. 7, no. 8, pp. 697–705, May 2013.

[27] T. J. Willink, C. C. Squires, G. W. K. Colman, and M. T. Muccio, "Measurement and characterization of low-altitude air-to-ground MIMO channels," *IEEE Trans. on Veh. Tech.*, vol. 65, no. 4, pp. 2637–2648, Apr. 2016.

[28] T. J. Harris and M. L. Scholz, "Characterisation of narrowband HF channels in the mid and low latitude ionosphere," Defence Sci. and Tech. Org., Australia, Tech. Rep., 2006.

[29] D. C. Cox, "A measured delay-Doppler scattering function for multipath propagation at 910 MHz in an urban mobile radio environment," *Proc. of the IEEE*, vol. 61, no. 4, pp. 479–480, 1973.

[30] L. S. Wagner, J. A. Goldstein, W. D. Meyer, and P. A. Bello, "The HF skywave channel: measured scattering functions for midlatitude and auroral channels and estimates for short term wideband HF rake modem performance," in *Proc. IEEE Conf. Mil. Commun. (MILCOM)*, vol. 3, 1989, pp. 830–839.

[31] E. E. Johnson, E. Koski, W. N. Furman, M. Jorgenson, and J. Nieto, *Third-generation and wideband HF radio communications.* Artech House, 2013.

[32] C. Lamy-Bergot, J.-B. Chantelouve, J.-Y. Bernier, H. Diakhaté, and J.-L. Rogier, "HF XL: adaptive wideband HF transmissions," in *Nordic HF Conf*, 2013, pp. 12–14.

[33] O. J. Smith, M. J. Angling, P. S. Cannon, V. Jodalen, B. Jacobsen, and O. K. Gronnerud, "Simultaneous measurements of propagation characteristics on non contiguous HF channels," in *Conf. Ant. and Propag.*, 2001, pp. 383–387.

[34] C. Watterson, J. Juroshek, and W. Bensema, "Experimental confirmation of an HF channel model," *IEEE Trans. on Commun. Tech.*, vol. 18, no. 6, pp. 792–803, Dec. 1970.

[35] NATO, "STANAG 4415: Characteristics of a robust, non-hopping, serial tone modulator/demodulator for severely degraded HF radio links," available at standards.globalspec.com/std/246230/nato-stanag-4415. Accessed June 12, 2018.

[36] NATO, "STANAG 4539: Technical Standards for non-hopping HF communications waveforms," available at standards.globalspec.com/std/1019095/nato-stanag-4539. Accessed June 12, 2018.

[37] NATO, "STANAG 4538: Technical Standards for an Automatic Radio Control System (ARCS) for HF communication links," available at standards.globalspec.com/std/1266944/nato-stanag-4538. Accessed June 12, 2018.

[38] M. J. Angling, P. S. Cannon, N. C. Davies, T. J. Willink, V. Jodalen, and B. Lundborg, "Measurements of Doppler and multipath spread on oblique

high-latitude Hf paths and their use in characterizing data modem performance," *Radio Sci.*, vol. 33, no. 1, pp. 97–107, 1998.

[39] T. J. Willink, "Analysis of high-latitude HF propagation characteristics and their impact for data communications," Communications Research Centre Canada, Tech. Rep. 97-001, Apr. 1997.

[40] B. A. Witvliet and R. M. Alsina-Pagès, "Radio communication via near vertical incidence skywave propagation: an overview," *Teecommunication Systems*, vol. 66, no. 2, pp. 295–309, Oct. 2017.

[41] V. Jodalen, B. Lundborg, and B. Jacobsen, "Channel characteristics of HF NVIS paths in northern Scandinavia," in *Proc. HF Radio Systems and Techn.*, Jul. 2000.

[42] T. J. Willink, "Modal power considerations in modem performance evaluation," in *Proc. of Nordic Shortwave Conference*, Aug. 1998.

[43] T. Willink, "DAMSON analysis for ARCS," Communications Research Centre, Tech. Rep. VPRB 05/96, Nov. 1996.

[44] T. J. Willink, "Wide-sense stationarity of mobile MIMO radio channels," *IEEE Trans. on Veh. Tech.*, vol. 57, no. 2, pp. 704–714, Mar. 2008.

[45] P. Bello, "Characterization of randomly time-variant linear channels," *IEEE Trans. on Commun. Sys.*, vol. 11, no. 4, pp. 360–393, Dec. 1963.

[46] A. Papoulis, *Probability, random variables, and stochastic processes.* McGraw-Hill, 1984.

[47] R. Barker, *Group Synchronizing of Binary Digital Systems*, W. Jackson, Ed. Academic-Butterworth, 1953.

[48] N. Zhang and S. Golomb, "Sixty-phase generalized Barker sequences," *IEEE Trans. Inform. Theory*, vol. IT-35, pp. 911–912, 1989.

[49] U. Somaini and M. Ackroyd, "Uniform complex codes with low autocorrelation sidelobes," *IEEE Trans. Inform. Theory*, vol. IT-20, pp. 689–691, Sept. 1974.

[50] D. Huffman, "The generation of impulse-equivalent pulse trains," *IRE Trans. Inform. Theory*, vol. 8, no. 5, pp. 10–16, Sep. 1962.

[51] M. Antweiler and L. Bömer, "Merit factor of Chu and Frank sequences," *Elect. Lett.*, vol. 26, no. 25, pp. 2068–2070, Dec. 1990.

[52] T. J. Willink, "Improving power allocation to MIMO eigenbeams under imperfect channel estimation," *IEEE Commun. Lett*, vol. 9, no. 7, pp. 622–624, Jul. 2005.

[53] S. O. Rice, "Mathematical analysis of random noise," *The Bell System Technical Journal*, vol. 24, no. 1, pp. 46–156, 1945.

[54] M. J. Gans, "A power-spectral theory of propagation in the mobile-radio environment," *IEEE Trans. Veh. Technol.*, vol. 21, no. 1, pp. 27–38, 1972.

[55] D. Cox and R. Leck, "Correlation bandwidth and delay spread multipath propagation statistics for 910-MHz urban mobile radio channels," *IEEE Trans. Commun.*, vol. 23, no. 11, pp. 1271–1280, 1975.

[56] A. F. Molisch, *Wireless communications.* John Wiley & Sons, 2012.

# Annex A Candidate sequences

## A.1 Complex aperiodic sequences

The complex uniform sequences can be defined by the phases of each symbol. The phases $\theta_k$ for the complex Barker, Somaini and FZC sequences are shown below. They are transmitted using

$$s_k = e^{j\theta_k} \tag{A.1}$$

***Table A.1:*** *Phase of elements of Barker 25 sequence.*

| | | | | |
|---|---|---|---|---|
| 2.625 | 2.958 | 1.861 | 2.489 | 4.719 |
| 5.805 | 5.209 | 5.306 | 4.192 | 5.292 |
| 1.231 | 2.828 | 4.894 | 4.740 | 3.679 |
| 1.494 | 6.101 | 3.555 | 3.457 | 6.114 |
| 3.446 | 0.614 | 4.014 | 1.417 | 4.250 |

***Table A.2:*** *Phase of elements of Somaini 13 sequence.*

| | | | | | |
|---|---|---|---|---|---|
| 1.617 | 5.850 | 1.622 | 5.907 | 1.228 | 6.110 |
| 5.466 | 2.815 | 1.254 | 1.162 | 2.885 | 4.423 |
| 5.515 | | | | | |

***Table A.3:*** *Phase of elements of Somaini 25 sequence.*

| | | | | |
|---|---|---|---|---|
| 2.545 | 2.825 | 1.945 | 2.625 | 4.946 |
| 5.826 | 5.146 | 5.108 | 4.106 | 5.346 |
| 1.105 | 3.025 | 4.946 | 4.786 | 3.626 |
| 1.505 | 6.148 | 3.666 | 3.386 | 0.025 |
| 3.506 | 0.425 | 3.866 | 1.505 | 4.066 |

***Table A.4:*** *Phase of elements of Somaini 64 sequence.*

| | | | | | |
|---|---|---|---|---|---|
| 0.040 | 0.480 | 0.440 | 0.240 | 0.360 | 0.120 |
| 0.200 | 0 | 0.280 | 1.065 | 2.071 | 3.317 |
| 3.741 | 4.247 | 4.752 | 5.698 | 0.720 | 1.971 |
| 3.461 | 5.512 | 0.920 | 1.731 | 3.421 | 4.912 |
| 0.240 | 2.796 | 5.672 | 1.345 | 3.661 | 6.138 |
| 1.571 | 3.767 | 0.040 | 3.141 | 0.200 | 3.261 |
| 6.083 | 2.980 | 6.243 | 2.660 | 5.923 | 3.567 |
| 1.491 | 5.738 | 3.221 | 0.265 | 4.312 | 1.876 |
| 6.203 | 4.472 | 3.221 | 1.691 | 0.200 | 4.192 |
| 2.340 | 1.451 | 0.320 | 6.018 | 5.272 | 4.447 |
| 3.621 | 2.966 | 1.851 | 0.385 | | |

***Table A.5:*** *Phase of FZC 30 sequence elements.*

| | | | | | |
|---|---|---|---|---|---|
| 0 | 6.178 | 5.864 | 5.341 | 4.608 | 3.665 |
| 2.513 | 1.152 | 5.864 | 4.084 | 2.094 | 6.178 |
| 3.770 | 1.152 | 4.608 | 1.571 | 4.608 | 1.152 |
| 3.770 | 6.178 | 2.094 | 4.084 | 5.864 | 1.152 |
| 2.513 | 3.665 | 4.608 | 5.341 | 5.864 | 6.178 |

***Table A.6:*** *Phase of FZC 60 sequence elements.*

| | | | | | |
|---|---|---|---|---|---|
| 0 | 6.231 | 6.074 | 5.812 | 5.445 | 4.974 |
| 4.398 | 3.718 | 2.932 | 2.042 | 1.047 | 6.231 |
| 5.027 | 3.718 | 2.304 | 0.785 | 5.445 | 3.718 |
| 1.885 | 6.231 | 4.189 | 2.042 | 6.074 | 3.718 |
| 1.257 | 4.974 | 2.304 | 5.812 | 2.932 | 6.231 |
| 3.142 | 6.231 | 2.932 | 5.812 | 2.304 | 4.974 |
| 1.257 | 3.718 | 6.074 | 2.042 | 4.189 | 6.231 |
| 1.885 | 3.718 | 5.445 | 0.785 | 2.304 | 3.718 |
| 5.027 | 6.231 | 1.047 | 2.042 | 2.932 | 3.718 |
| 4.398 | 4.974 | 5.445 | 5.812 | 6.074 | 6.231 |

## A.2 Real non-uniform sequences

The real non-uniform sequences are defined by the amplitudes of each symbol. The amplitudes for the two Huffman sequences used are given below.

***Table A.7:*** *Huffman 35 sequence elements.*

| | | | | |
|---|---|---|---|---|
| 1 | 1.200 | 0.720 | 1.632 | 1.699 |
| 2.652 | 3.290 | 4.626 | 6.065 | 8.265 |
| 11.024 | 14.879 | 19.952 | 26.851 | 36.063 |
| 48.488 | 65.155 | -64.802 | -65.155 | 48.488 |
| -36.063 | 26.851 | -19.952 | 14.879 | -11.024 |
| 8.265 | -6.065 | 4.626 | -3.290 | 2.652 |
| -1.699 | 1.632 | -0.720 | 1.200 | -1 |

***Table A.8:*** *Huffman 51 sequence elements.*

| | | | | | |
|---|---|---|---|---|---|
| 1 | 1.200 | 0.720 | 1.632 | 1.699 | 2.652 |
| 3.290 | 4.626 | 6.065 | 8.265 | 11.024 | 14.879 |
| 19.952 | 26.851 | 36.063 | 48.488 | 65.155 | 87.582 |
| 117.704 | 158.204 | 212.627 | 285.780 | 384.095 | 516.237 |
| 693.838 | -690.126 | -693.838 | 516.237 | -384.095 | 285.780 |
| -212.627 | 158.204 | -117.704 | 87.582 | -65.155 | 48.488 |
| -36.063 | 26.851 | -19.952 | 14.879 | -11.024 | 8.265 |
| -6.065 | 4.626 | -3.290 | 2.652 | -1.699 | 1.632 |
| -0.720 | 1.200 | -1 | | | |

## A.3 Periodic sequences

The m-sequences are generated using a shift register as illustrated in Figure 3, using the following taps:

**m-sequence 7** taps [3 2];

**m-sequence 15** taps [4 3];

**m-sequence 31** taps [5 4 3 1];

**m-sequence 63** taps [6 5 4 1].

## DOCUMENT CONTROL DATA

*Security markings for the title, authors, abstract and keywords must be entered when the document is sensitive

| | |
|---|---|
| 1. ORIGINATOR (Name and address of the organization preparing the document. A DRDC Centre sponsoring a contractor's report, or a tasking agency, is entered in Section 8.)<br>DRDC – Ottawa Research Centre<br>3701 Carling Avenue, Ottawa ON  K1A 0Z4, Canada | 2a. SECURITY MARKING (Overall security marking of the document, including supplemental markings if applicable.)<br>CAN UNCLASSIFIED<br><br>2b. CONTROLLED GOODS<br>NON-CONTROLLED GOODS<br>DMC A |

3. TITLE (The document title and sub-title as indicated on the title page.)

Sounding principles for high latitude BLOS HF channels

4. AUTHORS (Last name, followed by initials – ranks, titles, etc. not to be used. Use semi-colon as delimiter)

Willink, T. J.

| 5. DATE OF PUBLICATION (Month and year of publication of document.) | 6a. NO. OF PAGES (Total pages, including Annexes, excluding DCD, covering and verso pages.) | 6b. NO. OF REFS (Total cited in document.) |
|---|---|---|
| November 2018 | 44 | 56 |

7. DOCUMENT CATEGORY (e.g., Scientific Report, Contract Report, Scientific Letter)

Reference Document

8. SPONSORING CENTRE (The name and address of the department project or laboratory sponsoring the research and development.)

DRDC – Ottawa Research Centre
3701 Carling Avenue, Ottawa ON  K1A 0Z4, Canada

| 9a. PROJECT OR GRANT NO. (If appropriate, the applicable research and development project or grant number under which the document was written. Please specify whether project or grant.) | 9b. CONTRACT NO. (If appropriate, the applicable contract number under which the document was written.) |
|---|---|
| 05 | |

| 10a. DRDC DOCUMENT NUMBER | 10b. OTHER DOCUMENT NO(s). (Any other numbers which may be assigned this document either by the originator or by the sponsor.) |
|---|---|
| DRDC-RDDC-2018-D122 | |

11a. FUTURE DISTRIBUTION WITHIN CANADA (Approval for further dissemination of the document. Security classification must also be considered.)

Public release

11b. FUTURE DISTRIBUTION OUTSIDE CANADA (Approval for further dissemination of the document. Security classification must also be considered.)

Public release

12. KEYWORDS, DESCRIPTORS or IDENTIFIERS (Use semi-colon as a delimiter.)

HF communications; BLOS; propagation

13. ABSTRACT/RÉSUMÉ (When available in the document, the French version of the abstract must be included here.)

Beyond-line-of-sight (BLOS) HF communication propagates via the ionosphere; this atmospheric layer is disturbed by geomagnetic activity, causing the received signal to be distorted by Doppler fading and shift. In polar and auroral regions, these Doppler effects can be quite severe, affecting the reliability and robustness of communication links. Temporal dispersion causes multipath spread on each mode, and multiple modes may be observed resulting from reflection at different ionospheric layers and/or multi-hop paths that include reflection from the Earth. The propagation parameters are quite dynamic, with trends observed diurnally, seasonally and over the multi-year sunspot cycle, and vary by operating frequency. To design and evaluate radio technology for these conditions, it is necessary to characterise the propagation parameters on a variety of communication links at different times. Measurement campaigns to obtain the relevant ranges of parameters require carefully-designed channel sounders. Pseudo-noise sequences with pulse-compression characteristics are suitable for extracting the channel responses with a minimal amount of signal processing. Herein, several periodic and aperiodic pseudo-noise sequences are evaluated over a wide range of propagation conditions, obtained from previous high-latitude sounding campaigns. It is found that short aperiodic sequences are the most reliable selection: although they have limited processing gain, they are short enough to limit distortions due to Doppler fading and shift, and their implementation can be tuned to achieve appropriate trade-offs to measure the desired range of multipath and Doppler spreads. Other components to the sounding waveform might include capabilities to resolve ambiguities in delay and frequency.

Les communications HF (haute fréquence) au-delà de la ligne de visée se propagent grâce à l'ionosphère, une couche atmosphérique dont les perturbations dues à l'activité géomagnétique causent l'évanouissement et le décalage Doppler du signal. Ces effets Doppler peuvent être très intenses dans les régions polaires et aurorales et affecter ainsi la fiabilité et la constance des liens de communications. La dispersion temporelle crée un étalement causé par les trajets multiples pour chaque mode et on peut observer plusieurs modes produits par la réflexion sur différentes couches ionosphériques ou des trajets comportant plusieurs réflexions, notamment sur la Terre. Les paramètres de propagation sont donc plutôt dynamiques et on observe des tendances diurnes, saisonnières ou pendant le cycle solaire pluriannuel, et selon la fréquence utilisée. Pour concevoir et évaluer les technologies radio adaptées à ces conditions, il sera nécessaire de caractériser les paramètres de propagation pour un éventail de liens de communication à différents moments. Les campagnes de mesure visant à déterminer les différentes gammes de paramètres exigent des sondeurs de canaux conçus avec soin. Des séquences de pseudo bruit ayant des caractéristiques de compressions d'impulsions sont adéquates pour extraire les réponses des canaux tout en exigeant peu de traitement de signal. Le présent article contient notre évaluation des différentes séquences périodiques et apériodiques de pseudo bruit, pour un vaste éventail de conditions de propagation obtenues lors de campagnes antérieures de sondage à haute altitude. Nous avons trouvé que les séquences apériodiques courtes sont le choix le plus fiable : bien qu'elles présentent peu d'avantages en matière de traitement, elles sont suffisamment courtes pour limiter les distorsions causées par l'évanouissement et le décalage Doppler, et on peut ajuster leur utilisation pour obtenir des compromis permettant de mesurer la gamme désirée de trajets multiples et d'étalement Doppler. D'autres composants de la forme d'onde de sondage pourraient inclure la capacité de résoudre les ambiguïtés des retards et de fréquences.